https://doi.org/10.5194/egusphere-2024-1077
Preprint. Discussion started: 22 April 2024

Localized shear versus distributed strain accumulation as shear-accommodation mechanisms in ductile shear zones: Constraining their dictating factors

Pramit Chatterjee[1], Arnab Roy[1], and Nibir Mandal[1]

[1]Department of Geological Sciences, Jadavpur University, Kolkata 700032, India

Correspondence: Nibir Mandal (nibir.mandal@jadavpuruniversity.in)

Abstract. Understanding the underlying mechanisms of strain localization in Earth's lithosphere is crucial to explain the mechanics of tectonic plate boundaries and various failure-assisted geophysical phenomena, such as earthquakes. Geological observations suggest that ductile shear zones are the most important lithospheric structures of intense shear localization, sharing a major part of tectonic deformations. Despite extensive studies in the past several decades, the factors governing how they accommodate the bulk shear, whether by distributed homogeneous strain (i.e., development of S tectonic foliation normal to the principal shortening strain axis) or by localized shearing (formation of shear-parallel C bands) remain largely unexplored. This article aims to address this gap in knowledge, providing observational evidences of varying S and C development in ductile shear zones from two geological terrains of Eastern India. The field observations are complemented with 2D-viscoplastic numerical simulations within a strain-softening rheological framework to constrain the factors controlling the two competing shear-accommodation mechanisms: homogeneously distributed strain accumulation versus shear band formation. The model-based analysis recognizes the bulk shear rate ($\dot{\gamma_b}$), the bulk viscosity (η_v) and the initial cohesion (C_i) of a shear zone as the most critical factors to determine the dominance of one mechanism over the other. For a given C_i, low $\dot{\gamma_b}$ and η_v facilitate the formation of S foliation (uniformly distributed strain), which transforms to C-dominated shear-accommodation mechanism with increasing η_v. However, increasing $\dot{\gamma_b}$, facilitates shear accommodation in a combination of the two mechanisms leading to CS- structures. The article finally discusses the conditions in which ductile shear zones can enormously intensify localized shear rates to produce rapid slip events, such as frictional melting and seismic activities.

Keywords: deformation localization, shear accommodation mechanism, field analysis of shear structures, finite element modelling, viscoplastic rheology, rheological weakening and slip events

1 Introduction

Ductile shear zones are long, narrow regions of intense strain localization, relative to their surroundings, that accommodate large amounts of tectonic movements. They occur on varied scales, ranging from grain (millimetres) to crustal scales (hundreds of kilometres) and at varying depths, covering upper crust to the upper mantle region (Adam et al., 2005; Vauchez et al., 2012; Fossen and Cavalcante, 2017). In Earth's lithospheric deformations large-scale shear zones often play a critical role in triggering catastrophic phenomena, such as fault-driven earthquakes (Fagereng et al., 2014; French and Condit, 2019; Kotowski and Behr, 2019; Beall et al., 2021; Rodriguez Padilla et al., 2022), landslides (Korup et al., 2007; Hughes et al., 2020) and abrupt topographic modifications (Malik et al., 2006; Wang et al., 2020; Rodriguez Padilla, 2023). They also act as potential locations for shear-induced partial melting of rocks, as widely documented from their association with pseudotachylytes (Sibson, 1975; Papa et al., 2023), which can dramatically augments fault-slip rates and associated strain accumulation process, leading to mega-earthquake events (Di Toro et al., 2006; Rice, 2006; Menegon et al., 2021). Understanding their internal shear-accommodation mechanisms has thus set a critical area of study in solid earth geophysics, especially with a special focus on the rheological contributions to shear enhancement processes. Both field and experimental observations suggest that ductile shear zones generally accommodate strain by contrasting micro-scale deformation mechanisms in brittle and ductile regimes (Fossen and Cavalcante, 2017), where grain scale fracturing, grain rotation and frictional sliding are the principal mechanisms in the brittle regime(Sibson, 1977; Logan, 1979), whereas dislocation-assisted creep (crystal-plastic), grain-boundary sliding and syn-kinematic recrystallization dominating mechanisms in the ductile regime (Passchier and Trouw, 2005). However, shear zones typically evolve through strain partitioning along macroscopic shear bands, irrespective of their internal deformation mechanisms, and these bands share a large fraction of the bulk shear in the shear zones.

The origin of shear bands in rocks and practical solid materials, such as metals and polymers has remained a subject of challenging studies over several decades, particularly in the context of failure analysis (Bowden and Raha, 1970; Wang and Lade, 2001; Torki and Benzerga, 2018; Finch et al., 2020; del Castillo et al., 2021). Compression test experiments on homogeneous isotropic solids show shear band localization in conjugate sets, with their dihedral angles varying in the range of 60° to 90°, depending on deformation conditions, such as the strain rate, and mechanical properties, such as coefficient of internal friction, dilatancy factor, strain hardening parameter(Bowden and Raha, 1970; Roscoe, 1970; Rudnicki and Rice, 1975; Vardoulakis et al., 1978; Anand and Spitzig, 1980, 1982; Wang and Lade, 2001; Kaus, 2010; Torki and Benzerga, 2018; Mukhopadhyay et al., 2023). Several theoretical models have predicted the shear band angles to the compression axis in isotropic materials as a function of the physical variables mentioned above (Hutchinson and Tvergaard, 1981; Anand and Su, 2005). Brittle-ductile layered composites also undergo failure in conjugate shear bands, although their modes of development switching from localized to distributed, with increasing brittle to ductile layer-thickness and viscosity ratios (Schueller et al., 2010). A similar line of failure studies focuses on the mechanisms of shear localization in simple shear deformation of granular rocks, which suggest that shear bands develop in a more complex manner, forming multiple sets, compared to a simple conjugate set of band formation under compressional deformations. The multiple shear bands in granular materials, described as Y-, B-, P- and R bands form at characteristic angles to the bulk shear direction (Logan, 1979; Logan et al., 1992) , where Y and B bands are oriented parallel to the shear direction (B bands localize preferentially at the shear zone boundaries), and P bands occur at an angle of 15°- 45°with their vergence in the shear direction. R (Riedel) constitutes the most dominant two sets of antithetically vergent shear bands, one set at low-angles ($\sim 15° - 20°$) and the other at high angles (60°- 70°) to the shear direction, conventionally symbolized as R_1 and R_2 bands, respectively (Roy et al., 2021). In shear deformations these secondary shear bands generally occur as discrete planar zones, often marked by localization of gouge materials with intense grain-size reduction (Volpe et al., 2022; Casas et al., 2023).

https://doi.org/10.5194/egusphere-2024-1077
Preprint. Discussion started: 22 April 2024

The mechanics of shear band formation in shear deformations is still a lively problem, which has rejuvenated fresh theoretical and experimental studies of shear failure in the last couple of decades (Fossen, 2010; Hall, 2013). Numerical shear experiments on granular materials suggest that shear bands localize shear not by any bifurcation of local mechanical states, but by a long-range geometrical interaction of material particles (Ord et al., 2007). On the other hand, Mair and (Mair and Abe, 2008) have demonstrated from 3D numerical simulations a direct correlation of strain localization with grain size reduction in fault gouge. Laboratory experiments have been conducted on quartz-feldspar-rich granular materials and carbonates (Logan, 1979; Marone and Scholz, 1989; Marone et al., 1990; Beeler et al., 1996). A direction of these experimental investigations suggests that the relative growth of multiple sets of bands depend significantly on phyllosilicate and water content in granular aggregates (Morgenstern and Tchalenko, 1967; Wijeyesekera and De Freitas, 1976; Maltman, 1977; Logan and Rauenzahn, 1987; Rutter et al., 1986; Logan et al., 1992; Saffer and Marone, 2003; Collettini et al., 2011; Haines et al., 2013; Giorgetti et al., 2015; Orellana et al., 2018; Okamoto et al., 2019; Ruggieri et al., 2021; Volpe et al., 2022). Shear deformation of ductile materials also produce secondary shear bands, as in brittle materials, and their studies have gained serious attention due to their implications in interpreting various geodynamic processes, such as lithospheric subduction, deformation-assisted fluid/melts migration and earthquake generation in ductile regimes (Katz et al., 2006; Kirkpatrick et al., 2021; Beall et al., 2021; Tulley et al., 2022; Mancktelow et al., 2022). The mode of strain accommodation in ductile shear zones, however, largely differ from those discussed above for granular brittle rheology. Although ductile materials typically accommodate shear by continuous deformations without any macroscopic fractures in shear zones Rutter et al. (1986), many authors have reported brittle features from ductile shear zones (Paterson and Wong, 2005; Fusseis et al., 2006; Fusseis and Handy, 2008; Mukherjee and Koyi, 2010; Doglioni et al., 2011; Meyer et al., 2017). Bercovici and Karato (2002) have shown theoretically strain localization in ductile lithosphere, taking into account the following three feedback mechanisms: thermal, damage, and grain-size feedback.

Extensive numerical and experimental modelling (Shimamoto, 1986, 1989; Burlini and Bruhn, 2005; Misra et al., 2009; Meyer et al., 2017; Finch et al., 2020) as well as field observations leads to a common finding that ductile shear zones accommodate their bulk shear deformation in two principal mechanisms: *uniformly distributed strain accumulation* and *localized shearing*. Distributed strain accumulation imparts pervasive planar fabrics (called S foliation in literature) tracking the XY plane of the finite strain ellipsoid, often defined by flattened grain shape and preferred orientations of phyllosilicates, e.g., muscovite, biotite, and chlorite. In contrast, localized shearing occur in spaced zones, forming shear bands either parallel or at low angles to the principal shear plane, commonly described as C and C' bands, respectively (Berthé et al., 1979; Bos and Spiers, 2001; Niemeijer and Spiers, 2005, 2006; Tesei et al., 2012, 2014). These bands accommodate large shear strains, compared to the surroundings, and they are characterized by extreme grain refinement. In some cases, shear bands (termed as C" bands) occur sporadically at high angles to the shear direction. Among these bands, C occurs as the most dominant structures in natural shear zones, and they develop as closely spaced planar zones to develop a foliation, as widely reported from typical SC mylonites in ductile shear zones, where the S and C foliations interact with one another, giving an anastomosing network structural characteristics in the sheared rocks. Some authors have described these fabrics also from brittle shear zones (Lin, 1999).

https://doi.org/10.5194/egusphere-2024-1077
Preprint. Discussion started: 22 April 2024

It follows from the preceding discussion that shear deformations in ductile shear zones generally occur by a combination of distributed viscous strain (homogeneous S foliation development) and localized plastic strain (shear band formation), but unequally (Lister and Snoke, 1984; Burlini and Bruhn, 2005; Mancktelow, 2006; Misra et al., 2009). Some ductile shear zones develop distributed viscous strains to produce penetrative planar fabrics, with little or no shear localization (Ramsay et al., 1983; Marques et al., 2013; Fossen and Cavalcante, 2017; Gomez-Rivas et al., 2017; Pennacchioni and Mancktelow, 2018), as often documented from shear zones with S mylonites, whereas another class of shear zones accommodate shear mainly by shear band formation with little or no distributed viscous strain (Lister and Snoke, 1984; Mukhopadhyay and Deb, 1995; Lloyd and Kendall, 2005), as reported from shear zones with dominantly C mylonites . What controls these two modes of shear accommodation is, however, less explored. In a recent study, Tokle et al. (2023) have addressed this problem from sheared quartzite, considering phyllosilicate content as a controlling factor, where phyllosilicates allow strains to localize preferentially in bands, leaving quartzite grains less deformed. Schueller et al. (2010) recognized composite structure of ductile and brittle layers and their viscosity ratio as factors to determine the distributed versus localized fracturing in shear zones. Numerical simulations have shown that the growth of macro shear bands or mesoscopic scale slip planes without any macroscopic localized bands in granular materials can form, depending on initial densities and loading paths (Darve et al., 2021). Despite these studies, the problem of distributed viscous strain versus localized shear band formation, especially in terms of a generalized rheological scheme needs further attention, which constitutes the central theme of this article.

To address this problem, the present study examines the modes (distributed strain accumulation versus localized shearing) of shear accommodation in ductile shear zones from the Chotonagpur Gneissic Complex and the Singbhum Shear Zone, East Indian cratons. The shear zones show spectacular variations in their structural features, based on which they are classified into three categories: i) shear zones dominated by C bands with weak penetrative S foliations, ii) shear zones dominated by S foliations, with some minor C bands, and iii) shear zones competing development of C bands and S foliations. We use numerical models to find the factors controlling the competing distributed strain versus localized shear accommodation mechanisms in them. The model results are presented to demonstrate that a combination of transient visco-plastic rheology, kinematic and geometric factors of ductile shear zones determine the mode of shear deformations. The article finally provides a map showing the fields of their growth as a function of two fundamental kinematic and rheological parameters: shear rate and viscosity, respectively. This study also discusses the shear-rate enhancement processes with their implications in underpinning the origin of slip-induced catastrophic processes, such as frictional melting and earthquakes in ductile regimes.

2 Field Observations

2.1 Study Area

We studied ductile shear zones in two tectonic regions of the Precambrian Craton: Singhbhum Shear zone (SSZ) and Chotanagpur Granite Gneissic Complex (CGGC) in Eastern India (Fig.1). A detailed description of their overall geological setting is presented in Supplementary (S1). The SSZ is a spectacular arcuate, about 200 km long and 2 km wide, thrust-type shear zone at the interface between the Archean nucleus on south and the North Singhbhum Mobile belt (NSMB). Our field investiga-

https://doi.org/10.5194/egusphere-2024-1077
Preprint. Discussion started: 22 April 2024

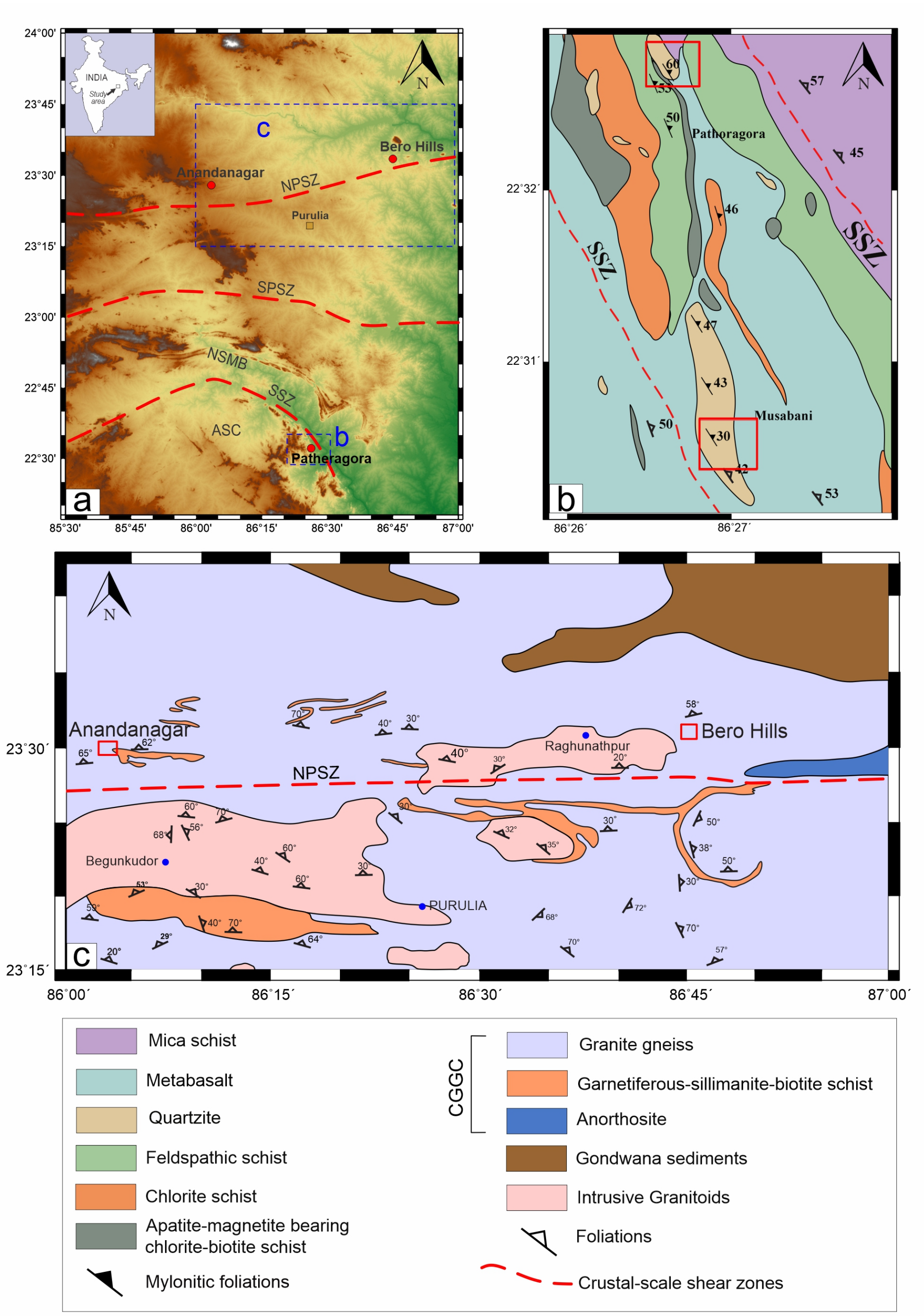

Figure 1. A simplified geological map of (a) the East Indian Precambrian craton, showing the dispositions of the Singhbhum Shear Zone (SSZ) and the Chotanagpur Granite Gneiss Complex (CGGC) (modified after Mukhopadhyay and Deb (1995); Mazumder et al. (2012); Roy et al. (2021, 2022)). Detailed geological maps of the two major study areas: (b) Pathoragora and Musabani region and (c) Purulia region. ASC: Archean Singhbhum Craton, NSMB: North Singhbbhum Mobile Belt, SPSZ: South Purulia shear zone, NPSZ: North Purulia shear zone.

https://doi.org/10.5194/egusphere-2024-1077
Preprint. Discussion started: 22 April 2024

tions in the SSZ concentrated in its south-eastern flank at Patheragora village (22°32′37.911"N, 86°26′31.223"E), near the old Surda copper mines and Musabani (22°30’59.3"N 86°26’26.5"E) town in Purbi Singhbhum district, Jharkhand. The main rock types of this area are quartzite mylonites, mica and chlorite schists, and mylonitised granite. The CGGC lies north of NSMB, covered mostly by a variety of granite gneisses, dotted with minor lithologies, e.g., mafic and ultramafic intrusives (Mahadevan, 1992). The host rocks are metamorphosed to amphibolite to granulite grades (Roy et al., 2021). We conducted our field investigations in the northern part of Purulia District at Bero hills (23°31’54.4"N 86°45’35.5"E) and Belamu Pahar in Anandanagar (23°27’56.1"N 86°03’26.6"E), where excellent outcrop-scale ductile shear zones are exposed in granite gneisses. They are typically a few centimeters to tens of meters long, with their thickness varying from a fraction of centimeters to several centimeters, often showing sharp deflections of steeply dipping across foliations in the host rocks. The CGGC shear zones mostly grew in simple shear strain with kinematical vorticity number W_k = 0.8 -1 (Dasgupta et al., 2015).

2.2 Macro-structural characteristics of SSZ rocks

Sheared quartzites in Pathoragora show closely spaced, macro-scale NE-dipping (20° to 60°) shear surfaces (C). Their exposed counterparts profusely contain down-dip slickenlines, indicating dominantly down-dip slip motion in the shear zones (Fig. 2a). At this location the macroscopic shear structures are characterized by a single set of parallel C surfaces, except some local gentle undulations. The C spacing varies on a wide range (2mm to 7cm). The sheared rocks are markedly devoid of S foliations on macroscale, as reported from Type II SC Mylonites by Lister and Snoke (1984). Sheared quartzites in Musabani area also show strongly developed C bands, marked by drastic grain size reduction (Fig. 2c and d). The band structures always dip in the NE direction, however, with varying magnitudes, from gentle (∼20°) to steep (∼45°) dips. They are laterally quite persistent, where a single C band is traceable over several meters in the down-dip as well as strike directions. The C bands are heterogeneously developed in the sheared rock, resulting in a strong variation in their spatial density (3.93 to 183.15) (Fig. 2b and c). Extremely close-spaced C-bands in places give rise to the appearance of a typical penetrative foliation, as widely reported from C-mylonites (Fig. 2d). We measured the C spacing, normalized to the effective local shear zone thickness, as indicator of rheology, which will be discussed later (Section 2.4). Macroscopic S foliations are characteristically absent in the sheared quartzites.

2.3 *Shear zones in CGGC and their internal structures*

Field investigations at Bero hills revealed sub-vertical shear zones in a granite gneiss at varied scales, with their thickness ranging from a few centimeters to more than a meter and their lengths extending up to tens of meters. Their internal structures are constituted by a combination of spaced C bands and penetrative S foliations, consistently forming angular relationship between them (Fig. 3). Individual C bands show varying thicknesses (2.7mm to 5.1cm) and the inter-band spacing also varies on a wide range (9cm to 1.8m). The bands are typically characterized by grain size reduction, which could be detected macroscopically in the field. In places, they contain undeformed elongate pods of the host rock as remnant masses, with their long directions oriented along the bulk shear plane. The shear zones have extensively developed penetrative foliations at angles to the shear zone boundary, often forming an anastomosing network with the C bands. This distributed foliation forms the lowest

https://doi.org/10.5194/egusphere-2024-1077
Preprint. Discussion started: 22 April 2024

Figure 2. : Field examples of C dominated ductile shear zones hosted in quartzites observed in Pathoragora and Musabani areas of SSZ. Notice strongly developed sub-parallel to parallel C-shear bands with varying spatial band density. (a) Slickenlines observed on the C surfaces indicating slip along these planes, (b-d) Intense shear localization along C bands of varying spatial densities. The bands are characterized by marked grain size reduction.SZ: Shear Zone.

angle with C bands close to the band structure, which increases away from the shear band. The average angle of foliation to the principal shear direction in this location varies in the range of 15° to 30°. Some domains within a shear zone remained virtually undeformed, as reflected from the absence of C bands as well as distributed foliations. We evaluated the area of fabric development, calculated by normalizing with that of corresponding shear-zone domains, as a measure of distributed deformations in the shear zones. The calculated values range from 0.22 to 0.83, implying that the shear-accommodation mechanisms by distributed strain accumulation varies spatially in ductile shear zones. Most of the ductile shear zones in Anandanagar area localize preferentially in quartzo-feldspathic pegmatites (Fig. 4a-c), with their lengths ranging from a few centimetres to more than 100 m and thickness varying from a fraction of cm to tens of centimetres. Some of them are hosted in the porphyritic granite (Fig. 4d). Their internal structures are dominated by distributed S foliations, showing little or no macroscopic shear-parallel bands. They are generally devoid of any drag zone at their interface with the host rocks, barring a few locations where they show foliation drag and offset of across-shear zone minor veins. The shear zones in pegmatites show obliquely orientated

https://doi.org/10.5194/egusphere-2024-1077
Preprint. Discussion started: 22 April 2024

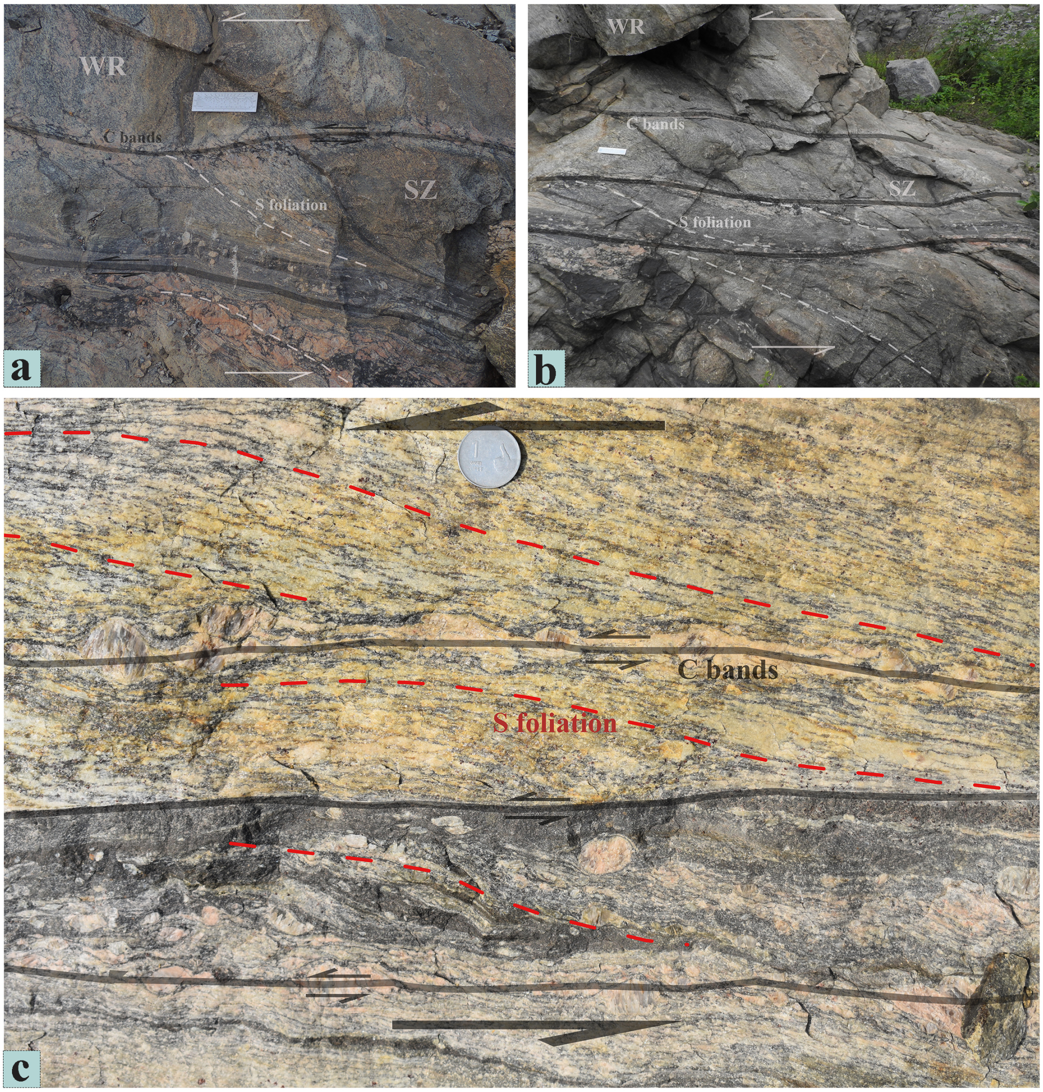

Figure 3. Outcrop-scale ductile shear zones containing penetrative S foliations in close association with widely spaced C bands; Bero Hills region of CGGC. (a - c) Sigmoidal patterns of S foliations in domains between C bands in the shear zone. The overall foliation trends occur persistently at an angle 20° to the C band direction. WR: Wall Rock; SZ: Shear Zone.

https://doi.org/10.5194/egusphere-2024-1077
Preprint. Discussion started: 22 April 2024

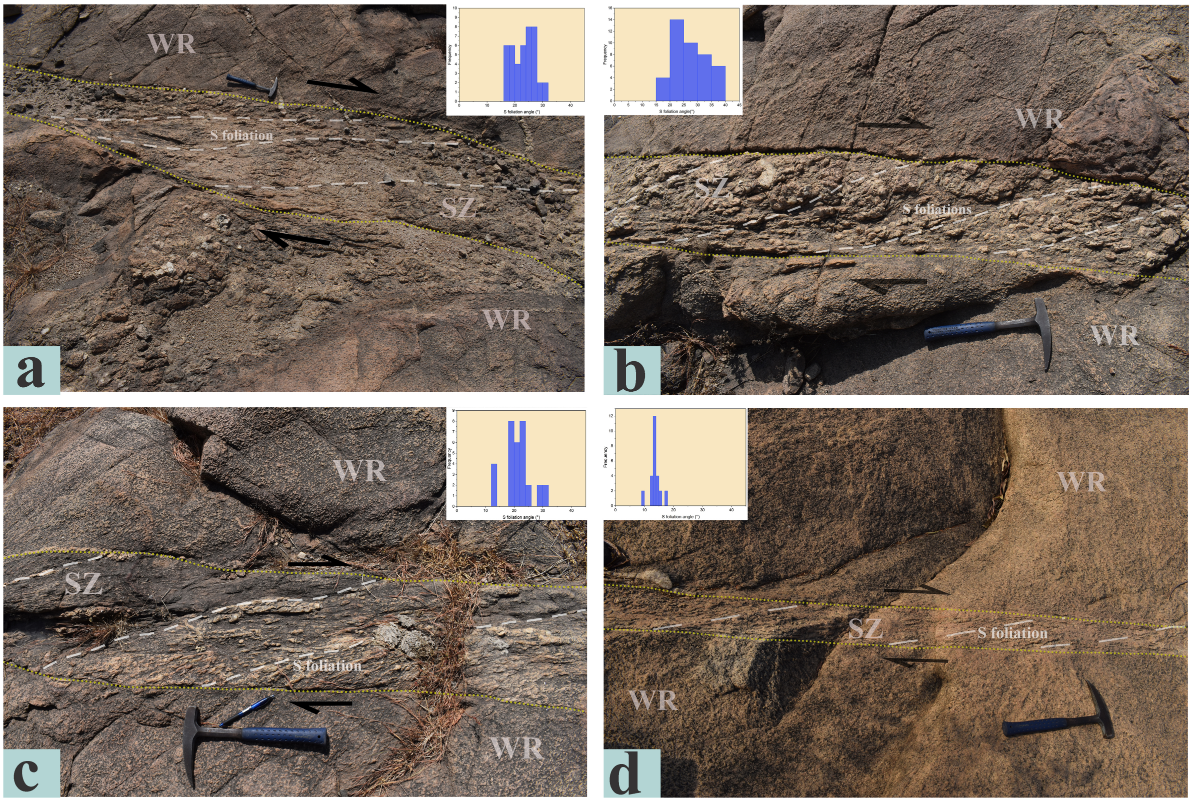

Figure 4. Field examples of S dominated ductile shear zones from Anandanagar area of the CGGC terrain. (a-d) Shear zones accommodating shear entirely by distributed strain accumulation, forming S foliations hosted. Notice complete absence of shear bands in them. Insets show the histogram plots of S foliation orientation (θ) with respect to the shear direction.WR: Wall Rock; SZ: Shear Zone.

penetrative S foliations at varying angles to their boundaries (15° to 35°). Assuming simple shear kinematics, the S-angles yield a finite shear strain of 1.6 in these shear zones. Shear zones in porphyritic granite similarly show obliquely oriented S foliations (Fig. 4d), leaving some protoliths of undeformed host rock within them. To summarize, shear zones in Anandanagar have accommodated shear dominantly by distributed strain (i.e., S foliation development), virtually with little C band-assisted deformation partitioning.

2.4 *A synthesis of the field observations*

The relative development of distributed S foliation and localized C bands in shear zones of our study areas (SSZ and CGGC), as described in the preceding section suggests two extreme shear accommodation mechanisms. In SSZ they accommodate shear through C band formation, whereas those in Anandanagar areas by distributed viscous deformation, with little or no macro-scale shear band formation. Some shear zones in CGGC have evolved in a hybrid mode, where the two mechanisms:

https://doi.org/10.5194/egusphere-2024-1077
Preprint. Discussion started: 22 April 2024

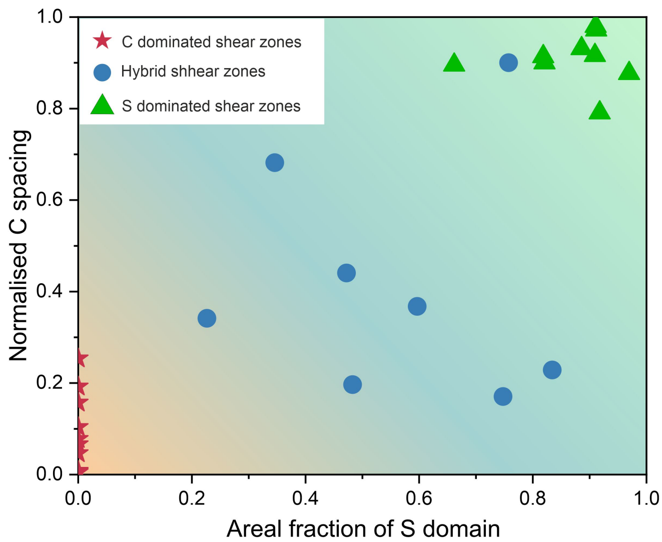

Figure 5. : Graphical plots of C band spacing versus areal fraction of S foliation domains. The plots delineate three distinct fields for S- and C-dominated, and hybrid shear zones. The data are collected from ductile shear zones in the CGGC and the SSZ. The C band spacing is normalized to shear zone thickness.

distributed viscous strain and localized C band formation operate equally. Based on the field data, we constructed a field diagram of shear zones with varying C versus S dominance using normalised C spacing and areal percentage of S foliation domains. C-dominated shear zones lie in the lower region of the field diagram while S-dominated shear zones (large areal percentage of S foliation) occupy the extreme right regime of the field diagram. The shear zone field data cluster to form distinct regions in the diagram (Fig. 5).

3 Numerical Modelling

3.1 Basic premises

The contrasting modes of shear accommodation revealed from our field observations are manifestations of varying kinematic and rheological conditions in the growth of ductile shear zones. To constrain their controls on the shear-accommodation mechanisms, we performed numerical simulations on model ductile shear zones, mechanically treated as narrow zones of viscous-plastic materials, undergoing Stokes flow, as applicable for incompressible slow, non-inertial viscous fluid flows (Gerya and Yuen, 2007; Jacquey and Cacace, 2020; Ranalli, 1997). The shear zone materials are assumed to yield plastically at threshold stresses. The model shear zones are approximated to crustal rheological regimes, setting their geometrical characteristics (e.g., length to thickness ratios) and kinematic conditions applicable to the corresponding natural prototypes.

https://doi.org/10.5194/egusphere-2024-1077
Preprint. Discussion started: 22 April 2024

3.2 Mathematical formulation

In our shear zone modelling, the mathematical formulation considers a two-layer system that embodies naturally formed shear zones, where a mechanically weak zone is hosted within a relatively stronger surrounding rock (wall) (Mancktelow, 2006; Pennacchioni and Mancktelow, 2018; Cawood and Platt, 2021). This modeling approach is effective for developing numerical, time-evolving, and dynamically consistent shear zone models in 2-D Cartesian domains within the theoretical framework of computational fluid dynamics (CFD). The CFD simulations, in this instance, assume an incompressible Boussinesq fluid flow, approximating the long-time (million years) scale kinematic state of Earth's lithospheric deformations. We employ the following continuity and momentum conservation equations in the CFD modelling:

$$\nabla . u_i = 0, \tag{1}$$

$$-\nabla P + \nabla \cdot \tau_{ij} + \ \rho g_i \ \ = 0 \tag{2}$$

where u denotes velocity, $P = 0.5(\sigma_{xx} + \sigma_{yy})$ is the pressure, τ is the deviatoric stress tensor, and g denotes gravitational acceleration. In Eq. (2), the inertial forces are neglected, as applicable to long-term flows in Earth's interior. The deviatoric stress tensor (τ_{ij}) is derived by subtracting the isotropic part from the total stress tensor (σ_{ij}). Assuming incompressible viscoplastic rheology, the deviatoric stress tensor (τ_{ij}) can be equated with the strain rate tensor as :

$$\tau_{ij} = 2\eta_{\text{eff}}\dot{\varepsilon}_{ij} = \eta_{\text{eff}} \left(\frac{\partial u_i}{\partial x_j} + \frac{\partial u_j}{\partial x_i} \right) \tag{3}$$

where $\dot{\varepsilon}_{ij}$ is the strain-rate tensor and η_{eff} is the effective viscosity, which includes viscosities η_v (viscous creep) and η_p (plastic creep) in their reciprocal form (Sandiford and Moresi, 2019) given as

$$\eta_{\text{eff}} = \frac{1}{\eta_v} + \frac{1}{\eta_p} \tag{4}$$

The shear zone modelling is implemented in an incompressible visco-plastic rheological framework (Ranalli, 1995), conventionally represented by a series connected frictional block – dashpot mechanical model. This consideration allows us to resolve the deviatoric strain-rate into two parts: viscous ($\dot{\varepsilon}^v_{ij}$), and plastic ($\dot{\varepsilon}^p_{ij}$) in the form

$$\dot{\varepsilon}_{ij} = \dot{\varepsilon}^v_{ij} + \dot{\varepsilon}^p_{ij} \tag{5}$$

where,

$$\dot{\varepsilon}^v_{ij} = \frac{1}{2}\frac{\tau_{ij}}{\eta_v} \qquad \dot{\varepsilon}^p_{ij} = \begin{cases} 0 & \text{if } J_2 < \sigma_{yield} \\ \chi \frac{\tau_{ij}}{2J_2} & \text{if } J_2 \geq \sigma_{yield} \end{cases} \tag{6}$$

$J_2 = 3(\sigma_{jj})^2 - \frac{1}{2}\sigma_{ij}\sigma_{ij}$ represents the second stress invariant, that determines the plastic creep at the yield point.

https://doi.org/10.5194/egusphere-2024-1077
Preprint. Discussion started: 22 April 2024

Natural shear zones accommodate shear mostly by large long-term permanent strains. Thus, the elastic (reversible) strain component is negligibly small ($\dot{\varepsilon}_{ij}^{e} \rightarrow 0$), as compared to the permanent viscous and plastic strains. Therefore, we ignore its effects on the shear zone models. Post-yield viscous weakening of the material is introduced, where the modified viscosity decreases non-linearly with increasing plastic strain. This rheological manipulation aims to develop strain-softening rheology in the shear zone models, which is implemented by equating the flow stress with the yield stress at the moment of yielding as

$$\eta_{\text{eff}} = \frac{\tau_{ij}}{2|\dot{\varepsilon}|} \tag{7}$$

To model shear zones formed at middle to lower crustal depths (Duretz et al., 2014; Gueydan et al., 2014; Reber et al., 2015), as applicable to our field studies, we have considered a linear relation of the yield stress (σ_{yield}) with pressure (P), and modelled the yield behaviour by employing a pressure-dependent plasticity (Drucker-Prager) criterion (Roy et al., 2021; Rast and Ruh, 2021). Based on this criterion, a yield function, F, can be defined in the following form

$$F = \sigma_{yield} - \sqrt{3}\sin(\phi)P - \sqrt{3}C(\gamma_{\text{pl}})\cos(\phi) \tag{8}$$

where $C(\gamma_{\text{pl}})$ is the material cohesion, expressed as a function of plastic strain γ_{pl}, and ϕ is the angle of internal friction. The cohesion is assumed to weaken with increasing accumulated plastic strain as,

$$C = C_i + (C_f - C_i)\min\left(1, \frac{\gamma_{\text{pl}}}{\gamma_o}\right) \tag{9}$$

where C_i is the initial cohesion and C_f is the final cohesion of the shear zone material. $\gamma_{\text{pl}} = \int_0^t \dot{\varepsilon}_p \, dt$ indicates accumulated plastic strain in regions where the yield limit is reached, and $\gamma_o = 0.1$ is taken as the reference strain. No syn-deformational healing of the cohesion is implemented in the present models.

3.3 Model Setup

Based on the mathematical formulation described in the preceding section, we developed 2D shear zone models using the open-source code Underworld 2 (http://www.underworldcode.org/) to solve the mass and momentum conservation equations (Eqs. 1 & 2) under incompressible conditions to obtain the pressure and velocity conditions within the shear zone domain. This code works within a continuum mechanics approximation, and has been extensively used to deal with a range of geological and geophysical problems (Beall et al., 2019; Mansour et al., 2020; Roy et al., 2024). As explained in Moresi et al. (2007) and Mansour et al. (2020), the code discretizes the geometrical domain into a standard Eulerian finite-element mesh and the domain is coupled with the particle-in-cell approach (Evans et al., 1957). To implement the particle-in-cell approach, the code discretizes the material domain into sets of Lagrangian material points, which allow us to find material properties that are history-dependent (in the present case, the plastic history of material) and can be tracked over the entire simulation run. Physical properties of the shear zone materials, such as density and viscosity are mapped by particle indexing. Our modelling excludes the effects of temperature diffusion and any inertia in the system.

The shear zone models were developed in a $4L \times L$ rectangular domain, where L represents the reference length scale. The model domain, occupied by incompressible visco-plastic materials, is discretized into quadrilateral mesh elements comprising

https://doi.org/10.5194/egusphere-2024-1077
Preprint. Discussion started: 22 April 2024

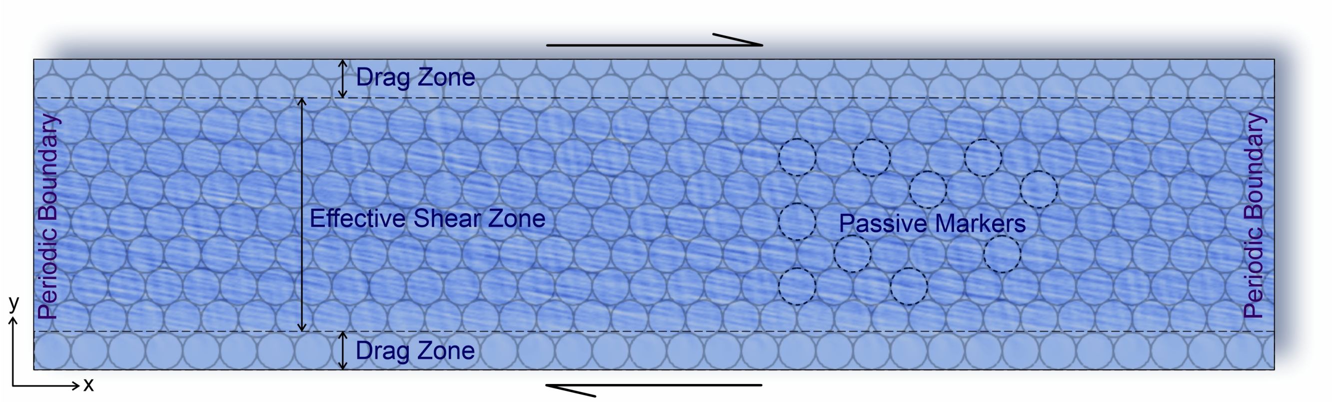

Figure 6. Representative initial shear zone model used for numerical simulation experiments run with a visco-plastic rheological approximation. The model considers a three-layered mechanical structure: a core, flanked by drag zones, hosted between two undeformable boundaries as commonly observed in geological settings. The model domain is imprinted with initially circular passive markers to determine the finite strain distributions across the shear zone. Further details of the model boundary conditions are provided in the text.

of 584×324 elements. We considered a three-layer model architecture (Roy et al., 2022) to simulate ductile shear zones, consisting of an intensely sheared core, flanked by drag zones on its either side, hosted in unsheared rocks, which structurally resemble those observed in the field (Fig. 2-4). The procedure to model the three-layered structure is discussed in detail in the Supplementary section S3. We imposed the following velocity boundary conditions in the shear zone models. The side model boundaries were subjected to a periodic boundary condition (Fig. 6), whereas the bottom and the top boundaries were assigned a prescribed velocity in the horizontal direction, keeping the overall strain rate constant throughout the simulation. The boundary velocities produced a dextral simple shear movement, where the maximum tensile stress (σ_1) axis is oriented at an angle of $45°$ to the bulk shear direction.

Our model simulations were run by varying the three major parameters: 1) bulk viscosity (η_v), 2) initial cohesion (C_i), and 3) bulk shear rates ($\dot{\gamma}_b$) in the system, where the first two characterize the rheology and the third represents the bulk kinematics of a shear zone. We vary η_v between $1\eta_o$ and $100\eta_o$, and similarly, $\dot{\gamma}_b$ between $1\dot{\gamma}_o$ and $100\dot{\gamma}_o$, where η_o and $\dot{\gamma}_o$ are the background viscosity and shear rate, respectively. All material parameters used in the simulations are summarized in Table 1.

3.4 Model shear zone characteristics

The simulations presented in this study primarily aim to constrain the rheological and kinematic conditions determining the shear accommodation mechanisms, leading to development of C, S, and C-S structures of ductile shear zones described from our field observations (Fig. 2-4). This section presents three sets of simulations to demonstrate the distinctive modes of strain evolution in model shear zones, designated as reference model (RM).

In the first set of RM1 simulations, run with $\eta_v = 1\eta_0$, $\dot{\gamma}_b = 0.5\dot{\gamma}_0$, and $C_i = 2C_0$, model shear zones accommodate the applied shear entirely by uniformly distributed continuous viscous deformations (Supplementary Video S1), revealed from

https://doi.org/10.5194/egusphere-2024-1077
Preprint. Discussion started: 22 April 2024

Table 1. Numerical model parameters and their values

Parameters	Symbol	Natural Values	Numerical Input Values
Model length	L	$4\ km$	4
Model width	W	$1\ km$	1
Model reference strain rate	$\dot{\gamma}_o$	$2.7e^{-14}\ s^{-1}$	1
Model reference density	ρg	$27000\ kgm^{-2}s^{-1}$	1
Model reference viscosity	η_0	$1e^{21}\ Pas$	1
Initial Cohesion	C_i	$27\ MPa$	1
Angle of friction	ϕ	$25° - 30°$	$25° - 30°$
Maximum Yield stress	σ_{max}	$1000\ MPa$	37
Minimum Yield stress	σ_{min}	$10\ MPa$	0.37

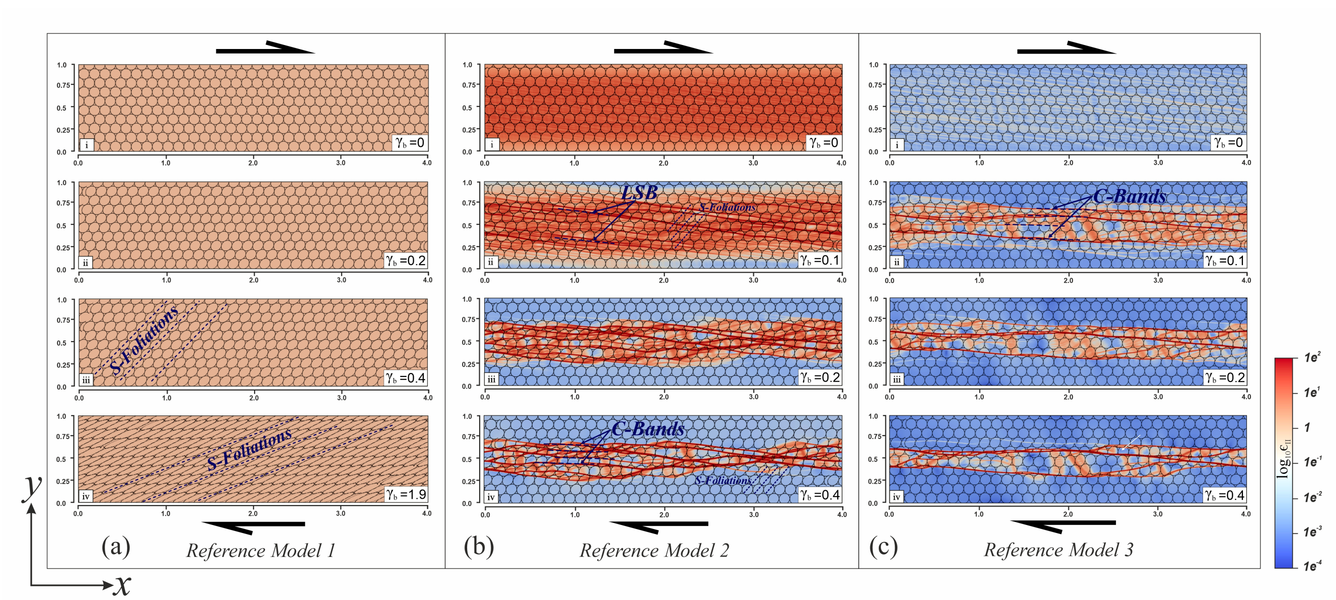

Figure 7. Evolution of ductile shear zones in the three reference models under dextral shear: (a) Reference model 1: $\eta_v = \eta_0$, $\dot{\gamma}_b = 0.5\dot{\gamma}_o$, and $C_i = 2C_0$ (b) Reference model 2: $\eta_v = 50\eta_0$, $\dot{\gamma}_b = 10\dot{\gamma}_o$, and $C_i = 1C_0$ (c) Reference model 3: $\eta_v = 100\eta_0$, $\dot{\gamma}_b = 3\dot{\gamma}_o$, and $C_i = 1C_0$, where η_0 and $\dot{\gamma}_o$ represent the background viscosity and shear rate, respectively. The color bar represents the logarithmic magnitude of strain rate invariant. Notice a transition of shear accommodation mechanism from homogeneously distributed strain accumulation to spaced shear band localization from RM 1 to 3. RM2 produces low-angle shear bands (LSB) in the initial stage of shear deformation ($\gamma_b < 0.2$), subsequently replaced by shear parallel C bands with progressive shearing movement.

https://doi.org/10.5194/egusphere-2024-1077
Preprint. Discussion started: 22 April 2024

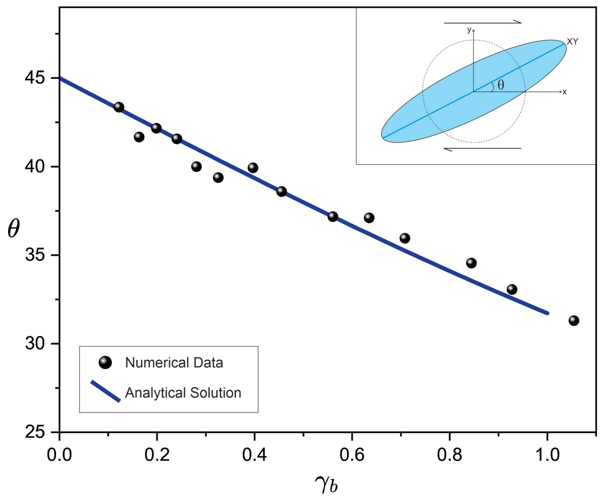

Figure 8. Inclinations (θ) of the major axis of finite strain ellipse (shown in inset) as a function of the finite shear (γ_b), obtained from RM1 numerical simulations (black dots). It is noteworthy that the numerical data regression agrees well with the analytical solution (solid blue line, Eq.10), implying that the model ductile shear zone has accommodated shear by homogeneously distributed strain accumulation.

deformed elliptical shapes of initially circular passive markers in the model (Fig. 7a-ii). The homogeneous strain continues to increase with progressive shear, but without showing any tendency to localize discernible shear bands throughout the simulation runtime (Fig. 7a-iv). Increasing finite bulk shear (γ_b) results in flattening of passive ellipses with decreasing inclinations of their major axes to the bulk shear direction in agreement with that obtained from homogeneous simple shear equation (Fig. 8):

$$\tan 2\theta = \frac{2}{\gamma_b} \quad (10)$$

This finding suggests that this type of model shear zones accommodate bulk shear entirely by homogeneous viscous strain, allowing no plastic yield-associated strain as the flow stress condition always lies below the yield point, which is evident from the clear absence of shear bands (Fig. 7a-iv). The RM1 simulations, consistently fail to produce shear band structures at any stage of shear zone evolution. Consequently, homogeneously distributed deformations emerge as the principal mechanism for accommodating shear.

The second reference model (RM2) simulations were run at high bulk shear rates ($\dot{\gamma}_b = 10\dot{\gamma}_o$) and high viscosity ($\eta_v = 50\eta_o$), while keeping $C_i = 1C_0$. At $\gamma_b = 0.09$, the RM2 simulation run developed finely spaced low-angle ($\theta \approx 13°$) shear bands and a few sporadic high-angle ($\theta \approx 85°$) shear bands (Supplementary Video S2). The densely packed low-angle bands impart a low-angle foliation in the ductile shear zone (Fig.7b-ii). Increase in γ_b gives rise to penetrative distributed viscous strains, revealed from elliptical shapes of the initially circular passive markers in the model, and the distributed strain accumulates steadily (Fig. 7b-ii) until γ_b reaches a threshold value (0.15) when the band structure underwent a drastic transformation with

https://doi.org/10.5194/egusphere-2024-1077
Preprint. Discussion started: 22 April 2024

the appearance of shear-parallel C bands at γ_b> 0.15 (Fig.7b-iii). The shear zone ultimately accommodates shear by a set of sub-parallel, wide-spaced ($\lambda^* =\sim 0.263$) C surfaces, forming a weak network, although locally with the earlier formed low-angle bands (Fig.7b-iv). P-bands localize sporadically, with a tendency to network with the principal C-bands. During the post-yield period the C-band assisted shearing becomes the dominant shear accommodation mechanism, manifested in disruption of the deformed passive markers (Fig. 7b-iv). The model shear zones thus accommodate the bulk shear initially by uniformly distributed viscous strain, switching to localized C band-assisted shear accommodation.

The third reference model (RM3) simulation is assigned an extremely high bulk viscosity ($\eta_v = 100\eta_o$) and a moderate bulk shear rate ($\dot{\gamma}_b = 3\dot{\gamma}_o$), produces a band growth pattern remarkably different from those observed in RM2 simulations (Supplementary Video S3). At $\gamma_b = 0.08$, the model first develops a set of low-angle shear bands at an angle of $\sim 15°$ to the shear direction, characterized by their narrow, long, and closely spaced ($\lambda \approx 0.006$) geometry, along with sporadically occurring thick high-angle shear bands ($\lambda \approx 0.19$). With progressively increasing bulk shear ($\gamma_b > 0.1$), shear band formation becomes the primary shear-accommodation mechanism, leading to a complete structural transformation into thick, widely spaced ($\lambda^* \approx 0.26$) shear-parallel C bands with virtually no traces of low-angle shear bands (Fig. 7c-ii). RM3 simulations show shear-zone evolution with little or no distributed viscous deformations, as indicated by the undeformed shapes of the initially circular markers in the model (Fig. 7c-iii). The post-yielding slip in the C-bands resulted in intense local deformations along the trace of these bands (Fig. 7c-iv). However, low-angle shear bands that formed at a low bulk shear ($\gamma_b < 0.1$) had little effect on the deformation of passive markers, implying that their slip was negligible.

3.5 C-band Localization versus Distributed Deformations: Rheological Constraints

Our simulation results reveal a functional relationship between the two distinct competing shear-accommodation mechanisms (distributed strain versus localized shearing) with the bulk shear rate ($\dot{\gamma}_b$) and the bulk viscosity (η_v) of ductile shear zones. The plotted data illustrates these relationships in a log-scale representation of $\dot{\gamma}^*(=\frac{\dot{\gamma}_b}{\dot{\gamma}_0})$ vs $\eta^*(=\frac{\eta_v}{\eta_0})$ space for a given value of $C_i = 1C_0$, where $\dot{\gamma}_0$ and η_0 are the background shear rate and viscosity, respectively, representing the regional shear rate and wall rock viscosity (see Fig. 9). The field diagram indicates that low $\dot{\gamma}_b$ and η_v values facilitate homogeneously distributed strain accumulation in the entire ductile shear zones. However, this mechanism is completely replaced by shear localization in the form of C-bands with increasing η_v. The field diagram also shows that increasing $\dot{\gamma}_b$ initially results in homogeneous strain-assisted shear accommodation, but once the yield point is surpassed, it switches to the C-band mechanism.

4 Discussion

4.1 Shear accommodation mechanisms and their crustal conditions

Field observations presented in Section 2 reveal contrasting structural characteristics in ductile shear zones in SSZ and CGGC. For example, sheared rocks in Anandanagar shear zones contain S foliations oblique to the shear zone boundaries with little or no macroscopic C bands, whereas those in Patherogora and Musabani extensively display shear parallel C bands, but no

https://doi.org/10.5194/egusphere-2024-1077
Preprint. Discussion started: 22 April 2024

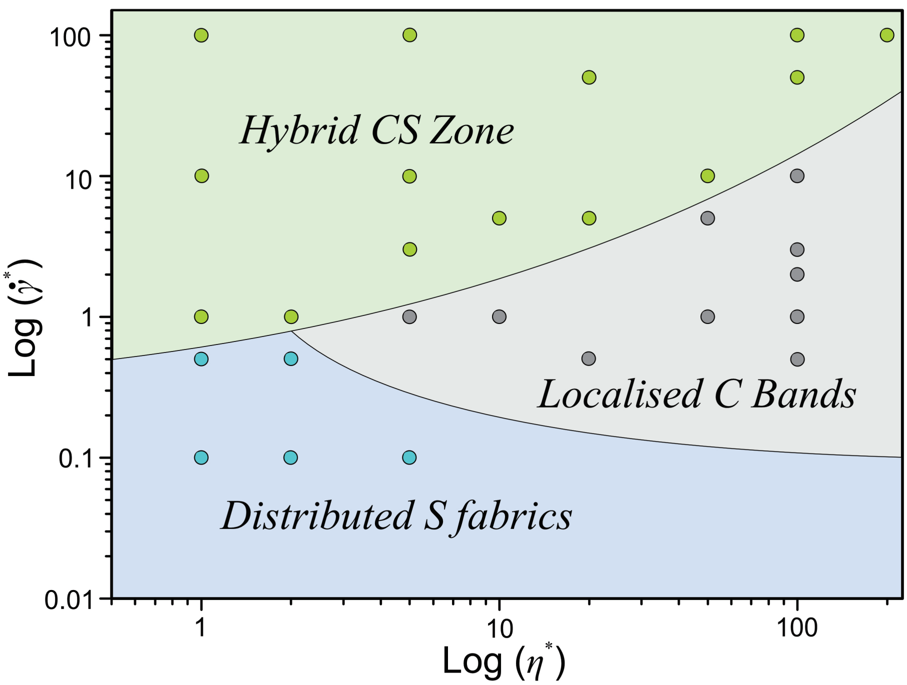

Figure 9. Field diagram of the three shear-accommodation mechanisms in a space defined by log-scale representation of γ^* ($\frac{\dot{\gamma}_b}{\dot{\gamma}_0}$) and η^* ($\frac{\eta_v}{\eta_0}$), constructed based on numerical simulations with $C_i = 1C_0$. $\dot{\gamma}_0$ and η_0 represent the background shear rate and viscosity in the regional setting. It is noteworthy that increasing initial bulk viscosity of ductile shear zone materials facilitates the C-band assisted shear-accommodation mechanism.

macroscopic S foliations. On the other hand, shear zones in Bero hills contain both the structural features. Modelling of ductile shear zones as incompressible viscous fluids with pressure sensitive plasticity suggest that these varying internal structural characteristics originate from their contrasting shear-accommodation mechanisms. S dominated ductile shear zones accommodate their bulk shear by spatially distributed viscous deformations across the whole shear zone, whereas those dominated by C bands accommodate shear by plastic strain localization, forming spaced shear bands.

These two end-member mechanisms of ductile shear zones are also manifested in their internal structural architectures. Shear zones are architecturally more homogeneous, showing uniformly developed S foliation in case of the first mechanism and geometrical continuity of across-shear zone passive markers, e.g., quartz veins. In contrast, the second mechanism results in heterogeneous structural architectures, characterized by a close association of localized zones of intense shearing, resulting in grain refinement and fluid assisted mineralisation along these zones, leaving adjoining regions relatively undeformed. Our numerical simulations indicate that low-strain rate crustal conditions favour the formation of internally homogeneous ductile shear zones by the first mechanism (Fig. 7a). In our study areas this type of shear zones occur in a tectonic setting of regional deformations within the CGGC terrain. Such internally homogeneous shear zones have also been extensively reported

https://doi.org/10.5194/egusphere-2024-1077
Preprint. Discussion started: 22 April 2024

from different geological terrains across the globe, e.g. Ramsay et al. (1983) Fossen and Cavalcante (2017) Pennacchioni and Mancktelow (2018). On the other hand, high strain-rate kinematic conditions, as applicable to specific crustal regimes, e.g. terrain boundaries and accretionary wedges in subduction zones, give rise to internally heterogeneous shear zones, characterized by strong strain partitioning in numerical simulations (Fig. 7c). Our model interpretations are consistent with the field observations from the Singhbhum Shear zone (SSZ), where the strain rates are expected to be high as the SSZ form the terrain boundary between the Proterozoic NSMB and the Archean Singhbhum craton (Ghosh and Sengupta, 1987). Several workers have shown evidences of slip and vein emplacement along shear surfaces in viscous shear zones from subduction margins (eg. Platt et al. (2018); Ujiie et al. (2018); Tulley et al. (2022). They often contain undeformed lenses formed by networking of anastomosing shear band structures (Carreras et al., 2010). These heterogeneities are generally attributed to fluid mediated mineralogical transformations along subducting plates or inherent lithological heterogeneities within the plate boundaries. Based on our numerical simulations, we propose that shear zones in initially mechanically homogeneous systems can evolve to become structurally heterogeneous due to the domination of shear-accommodation mechanisms by localized shearing, followed by various syn-shearing transformations, e.g., fluid-assisted mineral transformations.

Relative viscosity (η^*) and initial cohesion (C_i) of shear zone rocks also play a pivotal role in determining the internal architectural characteristics in our model shear zones. Low η^*, as observed in high-temperature environments at deep-crustal levels, favour a homogeneous structural characteristics of our model shear zones (Fig. 7a), which becomes extremely heterogeneous as η^* is increased to a threshold values ($\eta^* = 2$). In contrast, reducing cohesion, which may be assisted by syn-shearing micro-scale fracturing and fluid migration (Wu and Lavier, 2016; Menegon et al., 2021), can facilitate shear band formation, resulting in heterogeneous structures within the shear zones (Fig. 7b).

4.2 Mylonite characteristics: indicator of shear accommodation mechanisms

Mylonites are the typical representative rocks of ductile shear zones, produced by intense shearing and grain-size reduction, accompanying characteristic structural fabrics formation. Among them, C and S are most common planar fabrics in mylonites, as discussed in Section 1. However, field observations show wide variations in the relative development of these two fabrics, ranging from S- to C-dominated structures in mylonites, which are classified as Type I and II (Lister and Snoke, 1984). Although a broad spectrum of Type I and type II SC mylonites have been reported from natural ductile shear zones (Gates and Glover III, 1989; Mukhopadhyay and Deb, 1995; Cacciari et al., 2024), their origin deserves a discussion, especially in the context of shear localization mechanics. Our simulation results reveal that shear zones growing in high-viscosity rocks localize densely packed shear surfaces (Fig. 9) with little or no distributed homogeneous strain. This mechanical condition can thus produce shear parallel foliation without penetrative fabrics, as observed in ideal Type II mylonites. Lowering the bulk viscosity transforms the shear accommodation mechanism to facilitate the distributed strain accumulation setting (Fig. 9) a favourable condition for the development of selectively S fabrics, i.e., Type I mylonites. To summarize, the shear accommodation mechanism by shear band formation under high-viscosity conditions and/or high shear rate (Fig. 9) favours C-dominated mylonites (Type II), whereas that by distributed strain development under low-viscosity conditions with high strain rate (Fig. 9) facilitate Type I SC-mylonites in ductile shear zones.

https://doi.org/10.5194/egusphere-2024-1077
Preprint. Discussion started: 22 April 2024

A prolonged debate, which is still lively centres on the synchronous versus sequential development of S and C foliations in the evolution of shear zones. From field evidences Berthé et al. (1979) showed the coexistence of S and C at shear zone boundaries, both with their increasing spatial density towards the shear zone core. Their observation goes in favour of synchronous foliation development. However, this interpretation is not universally accepted and confronted with an alternative proposition, claiming that S foliations precede C localization. This structural sequence can occur when shear zones first accommodate shear by distributed strain, followed by plastic yielding to localize C surfaces. Lister and Snoke (1984) elaborated categorize mylonites into three types based on the temporal relationship between S and C fabrics. They showed that in some cases, both S and C foliations form synchronously in the same shear event, whereas in some other settings, e.g. an older metamorphic complex, they grow in two successive events, where S foliations formed in the earlier event are overprinted by C localization during the later deformation event. Their study finds a third possibility for a complex structural sequence, where transient flow patterns during ongoing shearing causes C foliations to align in the shortening field, leading to their folding and formation of a new set of S fabrics. Numerical simulations by Finch et al. (2020) and analogue experiments conducted by Dell'angelo and Tullis (1989) on quartzites provide additional insights. At low strain levels, the dominant foliations are primarily S foliations, with C' shear bands to form preferentially in the core regions of the shear zones, however, without distinct slip in highly strained samples. On the other hand, experiments conducted on quartz-feldspar aggregates produce weak S-C foliations, implying that monomineralic rocks, such as quartzite may not readily form S-C foliations. Burlini and Bruhn (2005) suggested distributed viscous strain and shear localization as the two competing processes. According to them, a brittle event occurs prior to onset of plastic yielding, otherwise the shear zone would develop distributed strain over the entire sample. Based on our numerical model results, we propose distributed viscous strain development and localized shearing as two end-member shear accommodation mechanisms, which can occur synchronously, although one dominating over the other depending on the rheological conditions of the shear zones. Consequently, a ductile shear zone can continue to accommodate viscous strain even after the C band formation or vice-versa in progressive shear.

4.3 Rheological controls and their tectonic implications

Earlier field and experimental investigations as well as numerical simulations have dealt with the problem of strain partitioning in polymineralic rocks, and demonstrate the distinctive roles of viscous and plastic strains in ductile shear zones (Mancktelow, 2006; Katz et al., 2006; Burlini and Bruhn, 2005; Misra et al., 2009; Finch et al., 2020; Tokle et al., 2023). The present study takes into account the pivotal effects of bulk rheology and kinematics on strain partitioning, and shows that the interplay of bulk viscosity, shear rate, and cohesion of materials within shear zones as the primary determining factors of shear zone processes. Depending on these factors, as discussed in the preceding section, shear zones undergo shearing entire by viscous strains with little or no internal shear localization that could produce porosity bands (Katz et al., 2006) to enhance the permeability in shear zones. In such situations they would hardly act as pathways for fluid or melt migration. In contrast, same shear zones can profusely produce shear bands under a favourable condition of the aforesaid factors that will provide effective permeability for fluid migrations, as often recorded in the form of shear-parallel veins and pegmatites (Creus et al., 2023; Koizumi et al., 2023). The role of ductile shear zones in deep-earth fluid transport processes, as shown by many authors (Cox, 2002; Fusseis et al., 2009; Spruzeniece and Piazolo, 2015; Précigout et al., 2017) thus depends primarily on the mode of shear zone evolution controlled by distributed strain versus localized shear accommodation mechanisms.

Several recent studies (Vissers et al., 2020; Allison and Dunham, 2021; Lavier et al., 2021; Mildon et al., 2022) have reported a number of phenomena, such as earthquake generation and frictional melting (pseudotachylites) from ductile shear zones that indicate the occurrence of extremely high shear rates, which are difficult to explain from relatively slow ductile shear kinematics. Evidently, there must be some weakening mechanisms in shear zone processes to amplify the shear rates by many orders, e.g., 10^{-12} s^{-1} to 10^{-3} s^{-1} (Kelemen and Hirth, 2004). Understanding the process of such shear rate enhancement is critically important to interpret many important deep-earth processes in ductile regimes, such as earthquakes within the subducting lithosphere, especially at depths ranging from 50 to 300 km. It is important to note that ductile mechanisms primarily govern deformation at high pressures and temperatures corresponding to such depths, and thus cannot account for seismic fault events (Platt et al., 2018; Gou et al., 2019). To address this problem, a range of explanations have been hypothesized for the mechanisms of intermediate-depth earthquakes, such as dehydration embrittlement and thermal runaway. Dehydration embrittlement, as proposed by Hacker et al. (2003) and Frohlich (2006), result from enhanced pore pressures, resulting from fluids released from metamorphic reactions. On the other hand, thermal runaway occurs due to interplay between weakening triggered by various factors and the temperature-dependent rock rheology (Kelemen and Hirth, 2007; Andersen et al., 2008; John et al., 2009; Braeck and Podladchikov, 2007; Thielmann and Kaus, 2012). Field evidence supporting thermal runaway includes the presence of pseudotachylites (e.g., Andersen et al. (2008); in fact, some of them are reported from ductile settings far below the brittle-ductile transition. Our study provides an alternative explanation for strain localization and strain-induced slip within ductile shear zones. Model results indicate that shear zones localize shear bands with significantly reduced effective viscosity. This strain softening phenomena are generally attributed to factors, such as grain size reduction, mineral reactions, and the development of crystallographic preferred orientation. The model shear bands locally enhance strain rates by ∼2-3 order. The viscoplastic model employed in this study incorporates a pressure-dependent yield criterion, contributing to strain localization along zones of strain softening(Fig. 10). We ran a set of simulation by increasing the degree of strain softening in this criterion to test how much softening is required to attain higher order strain rates. The simulation results showed that enormous shear rate enhancement along shear bands in the ductile regime must be accompanied by additional shear softening mechanisms e.g., porosity driven metamorphic fluids/melts can dramatically reduce the effective viscosity, as shown from theoretical calculations (Holtzman, 2016), where a small fraction ($\sim 5\%$) of melts/hydrothermal fluids can reduce the viscosity by an order of ∼2-3. We thus propose that ductile shear zones can produce earthquakes(Fig. 10) only when their evolution is modulated by the shear band-assisted shear-accommodation mechanism within a visco-plastic rheological condition, accompanying additional syn-shearing strain-softening enhancement agencies, such as fluids and melts.

https://doi.org/10.5194/egusphere-2024-1077
Preprint. Discussion started: 22 April 2024

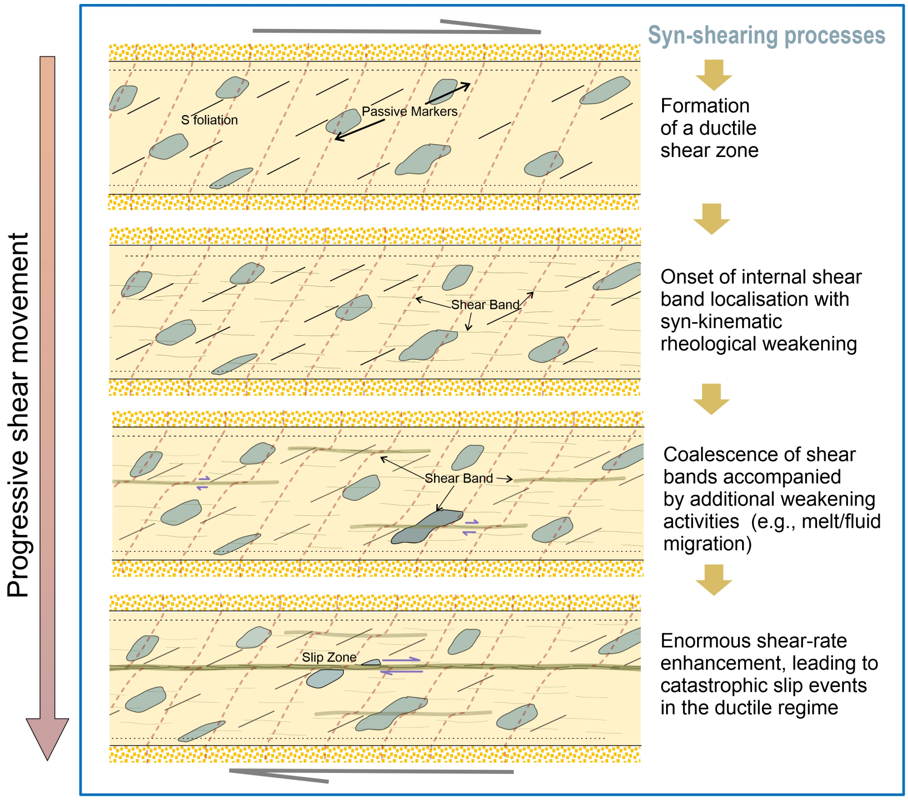

Figure 10. A visual representation illustrating various developmental phases of crustal-scale ductile shear zones subjected to dextral shear motion. The gradual escalation of shear, coupled with diverse syn-kinematic strain softening mechanisms, may culminate in catastrophic slip events within the ductile regime.

5 Conclusions

This study combines field observations and numerical simulations to show that shear-parallel strain localization and homogeneous viscous deformation as two competing mechanisms of deformation accommodation in ductile shear zones. We can summarise the findings along the following points.

a) Ductile shear zones produce strongly varying internal structural characteristics, modulated by the two competing shear-accommodation mechanisms. The localized shearing mechanism gives rise to shear-parallel band formation whereas distributed strain accumulations result in penetrative S foliation development tracking the XY plane of the finite strain ellipsoids.

b) These two competing mechanisms are controlled by the following three factors: bulk strain rate, bulk viscosity and initial cohesion. Increasing bulk viscosity and strain rate or reducing cohesive strength transform the shear accommodation mechanisms from distributed homogeneous strain accumulation to localized C band formation.

c) For a specific threshold of shear rate ($\dot{\gamma}^*$=0.5) under given viscosity and cohesion, ductile shear zones can produce both S foliations and C bands (e.g., SC mylonites) by distributed strain accumulation and localized shear-accommodation mechanisms, respectively.

d) Homogeneous versus heterogeneous internal architectural characteristics of shear zones hosted in an initially homogeneous rocks depend largely on the shear accommodation mechanisms. The distributed strain accumulation mechanism gives rise to more uniform structural architectures in low-strain ($\dot{\gamma}^* < 0.5$) crustal conditions, as compared to those produced by the localized shearing mechanism in high-strain ($\dot{\gamma}^* > 0.5$) crustal environments.

Code availability. The authors confirm that all the data used to support the findings of this study are available within the manuscript and as Supporting Information. All aspects of UNDERWORLD 2 (Beucher et al., 2022) can be downloaded and checked in this link: https://doi.org/10.5281/zenodo.6820562

.

Data availability. The relevant data supporting the conclusions are present in this manuscript, the Supporting Information and in the repository (https://doi.org/10.6084/m9.figshare.25563030) (Chatterjee et al., 2024)

.

Author contributions. PC conducted the field investigations, performed the analyses, and prepared the initial draft. AR conducted the numerical simulations and contributed to the initial draft writing. NM conceptualized the central research ideas and overall planning, supervised the methodologies, and revised the initial draft.

Competing interests. The authors declare that there are no conflict of interests.

Acknowledgements. PC acknowledges DST-SERB funded project(JBR/2022/000003) for providing doctoral research fellowship. AR gratefully acknowledges CSIR, India for awarding research fellowship grants (09/096(0940)/2018- EMR-I). The DST-SERB is acknowledged for supporting this work through the J.C. Bose fellowship (JBR/2022/000003) to NM.

References

Adam, J., Urai, J., Wieneke, B., Oncken, O., Pfeiffer, K., Kukowski, N., Lohrmann, J., Hoth, S., Van Der Zee, W., and Schmatz, J.: Shear localisation and strain distribution during tectonic faulting—New insights from granular-flow experiments and high-resolution optical image correlation techniques, Journal of Structural Geology, 27, 283–301, 2005.

Allison, K. L. and Dunham, E. M.: Influence of shear heating and thermomechanical coupling on earthquake sequences and the brittle-ductile transition, Journal of Geophysical Research: Solid Earth, 126, e2020JB021 394, 2021.

Anand, L. and Spitzig, W.: Initiation of localized shear bands in plane strain, Journal of the Mechanics and Physics of Solids, 28, 113–128, 1980.

Anand, L. and Spitzig, W.: Shear-band orientations in plane strain, Acta Metallurgica, 30, 553–561, 1982.

Anand, L. and Su, C.: A theory for amorphous viscoplastic materials undergoing finite deformations, with application to metallic glasses, Journal of the Mechanics and Physics of Solids, 53, 1362–1396, 2005.

Andersen, T. B., Mair, K., Austrheim, H., Podladchikov, Y. Y., and Vrijmoed, J. C.: Stress release in exhumed intermediate and deep earthquakes determined from ultramafic pseudotachylyte, Geology, 36, 995–998, 2008.

Beall, A., Fagereng, Å., and Ellis, S.: Fracture and weakening of jammed subduction shear zones, leading to the generation of slow slip events, Geochemistry, Geophysics, Geosystems, 20, 4869–4884, 2019.

Beall, A., Fagereng, Å., Davies, J. H., Garel, F., and Davies, D. R.: Influence of subduction zone dynamics on interface shear stress and potential relationship with seismogenic behavior, Geochemistry, Geophysics, Geosystems, 22, e2020GC009 267, 2021.

Beeler, N., Tullis, T., Blanpied, M., and Weeks, J.: Frictional behavior of large displacement experimental faults, Journal of Geophysical Research: Solid Earth, 101, 8697–8715, 1996.

Bercovici, D. and Karato, S.-i.: Theoretical analysis of shear localization in the lithosphere, Reviews in mineralogy and geochemistry, 51, 387–420, 2002.

Berthé, D., Choukroune, P., and Jégouzo, P.: Orthogneiss, mylonite and non coaxial deformation of granites: the example of the South Armorican Shear Zone, Journal of Structural Geology, 1, 31–42, 1979.

Beucher, R., Giordani, J., Moresi, L., Mansour, J., Kaluza, O., Velic, M., Farrington, R., Quenette, S., Beall, A., Sandiford, D., Mondy, L., Mallard, C., Rey, P., Duclaux, G., Laik, A., Morón, S., Beall, A., Knight, B., and Lu, N.: Underworld2: Python Geodynamics Modelling for Desktop, HPC and Cloud, https://doi.org/10.5281/zenodo.6820562, 2022.

Bos, B. and Spiers, C.: Experimental investigation into the microstructural and mechanical evolution of phyllosilicate-bearing fault rock under conditions favouring pressure solution, Journal of Structural Geology, 23, 1187–1202, 2001.

Bowden, P. and Raha, S.: The formation of micro shear bands in polystyrene and polymethylmethacrylate, The Philosophical Magazine: A Journal of Theoretical Experimental and Applied Physics, 22, 463–482, 1970.

Braeck, S. and Podladchikov, Y.: Spontaneous thermal runaway as an ultimate failure mechanism of materials, Physical Review Letters, 98, 095 504, 2007.

Burlini, L. and Bruhn, D.: High-strain zones: laboratory perspectives on strain softening during ductile deformation, Geological Society, London, Special Publications, 245, 1–24, 2005.

Cacciari, S., Pennacchioni, G., Cannaò, E., Scambelluri, M., and Toffol, G.: Fluid-rock interaction in eclogite-facies meta-peridotite (Erro-Tobbio Unit, Ligurian Alps, Italy), Tech. rep., Copernicus Meetings, 2024.

https://doi.org/10.5194/egusphere-2024-1077
Preprint. Discussion started: 22 April 2024

Carreras, J., Czeck, D. M., Druguet, E., and Hudleston, P. J.: Structure and development of an anastomosing network of ductile shear zones, Journal of Structural Geology, 32, 656–666, 2010.

Casas, N., Mollon, G., and Daouadji, A.: Influence of Grain-Scale Properties on Localization Patterns and Slip Weakening Within Dense Granular Fault Gouges, Journal of Geophysical Research: Solid Earth, 128, e2022JB025 666, 2023.

Cawood, T. and Platt, J.: What controls the width of ductile shear zones?, Tectonophysics, 816, 229 033, 2021.

Chatterjee, P., Roy, A., and Mandal, N.: Localized shear versus distributed strain accumulation as shear-accommodation mechanisms in ductile shear zones: Constraining their dictating factors, https://doi.org/10.6084/m9.figshare.25563030, 2024.

Collettini, C., Niemeijer, A., Viti, C., Smith, S. A., and Marone, C.: Fault structure, frictional properties and mixed-mode fault slip behavior, Earth and Planetary Science Letters, 311, 316–327, 2011.

Cox, S. F.: Fluid flow in mid-to deep crustal shear systems experimental constraints, observations on exhumed high fluid flux shear systems, and implications for seismogenic processes, Earth, planets and space, 54, 1121–1125, 2002.

Creus, P. K., Sanislav, I. V., Dirks, P. H., Jago, C. M., and Davis, B. K.: The Dugald River-type, shear zone hosted, Zn-Pb-Ag mineralisation, Mount Isa Inlier, Australia, Ore Geology Reviews, 155, https://doi.org/10.1016/j.oregeorev.2023.105369, 2023.

Darve, F., Nicot, F., Wautier, A., and Liu, J.: Slip lines versus shear bands: two competing localization modes, Mechanics Research Communications, 114, 103 603, 2021.

Dasgupta, S., Mandal, N., and Bose, S.: How far does a ductile shear zone permit transpression?, Ductile Shear Zones: From Micro-to Macro-scales, pp. 14–29, 2015.

del Castillo, E. M., Fávero Neto, A. H., and Borja, R. I.: Fault propagation and surface rupture in geologic materials with a meshfree continuum method, Acta Geotechnica, 16, 2463–2486, 2021.

Dell'angelo, L. N. and Tullis, J.: Fabric development in experimentally sheared quartzites, Tectonophysics, 169, 1–21, 1989.

Di Toro, G., Hirose, T., Nielsen, S., Pennacchioni, G., and Shimamoto, T.: Natural and experimental evidence of melt lubrication of faults during earthquakes, science, 311, 647–649, 2006.

Doglioni, C., Barba, S., Carminati, E., and Riguzzi, F.: Role of the brittle–ductile transition on fault activation, Physics of the Earth and Planetary Interiors, 184, 160–171, 2011.

Duretz, T., Schmalholz, S. M., Podladchikov, Y. Y., and Yuen, D. A.: Physics-controlled thickness of shear zones caused by viscous heating: Implications for crustal shear localization, Geophysical Research Letters, 41, 4904–4911, https://doi.org/10.1002/2014GL060438, 2014.

Evans, M. W., Harlow, F. H., and Bromberg, E.: The particle-in-cell method for hydrodynamic calculations, 1957.

Fagereng, Å., Hillary, G. W., and Diener, J. F.: Brittle-viscous deformation, slow slip, and tremor, Geophysical Research Letters, 41, 4159–4167, 2014.

Finch, M. A., Bons, P. D., Steinbach, F., Griera, A., Llorens, M. G., Gomez-Rivas, E., Ran, H., and de Riese, T.: The ephemeral development of C′ shear bands: A numerical modelling approach, Journal of Structural Geology, 139, https://doi.org/10.1016/j.jsg.2020.104091, 2020.

Fossen, H.: Deformation bands formed during soft-sediment deformation: observations from SE Utah, Marine and Petroleum Geology, 27, 215–222, 2010.

Fossen, H. and Cavalcante, G. C. G.: Shear zones–A review, Earth-Science Reviews, 171, 434–455, 2017.

French, M. E. and Condit, C. B.: Slip partitioning along an idealized subduction plate boundary at deep slow slip conditions, Earth and Planetary Science Letters, 528, 115 828, 2019.

Frohlich, C.: Deep earthquakes, 2006.

Fusseis, F. and Handy, M.: Micromechanisms of shear zone propagation at the brittle–viscous transition, Journal of Structural Geology, 30, 1242–1253, 2008.

Fusseis, F., Handy, M., and Schrank, C.: Networking of shear zones at the brittle-to-viscous transition (Cap de Creus, NE Spain), Journal of Structural Geology, 28, 1228–1243, 2006.

Fusseis, F., Regenauer-Lieb, K., Liu, J., Hough, R. M., and De Carlo, F.: Creep cavitation can establish a dynamic granular fluid pump in ductile shear zones, Nature, 459, 974–977, 2009.

Gates, A. E. and Glover III, L.: Alleghanian tectono-thermal evolution of the dextral transcurrent Hylas zone, Virginia Piedmont, USA, Journal of Structural Geology, 11, 407–419, 1989.

Gerya, T. V. and Yuen, D. A.: Robust characteristics method for modelling multiphase visco-elasto-plastic thermo-mechanical problems, Physics of the Earth and Planetary Interiors, 163, 83–105, 2007.

Ghosh, S. and Sengupta, S.: Progressive development of structures in a ductile shear zone, Journal of Structural Geology, 9, 277–287, 1987.

Giorgetti, C., Carpenter, B., and Collettini, C.: Frictional behavior of talc-calcite mixtures, Journal of Geophysical Research: Solid Earth, 120, 6614–6633, 2015.

Gomez-Rivas, E., Griera, A., Llorens, M.-G., Bons, P. D., Lebensohn, R. A., and Piazolo, S.: Subgrain rotation recrystallization during shearing: insights from full-field numerical simulations of halite polycrystals, Journal of Geophysical Research: Solid Earth, 122, 8810–8827, 2017.

Gou, T., Zhao, D., Huang, Z., and Wang, L.: Aseismic deep slab and mantle flow beneath Alaska: Insight from anisotropic tomography, Journal of Geophysical Research: Solid Earth, 124, 1700–1724, 2019.

Gueydan, F., Précigout, J., and Montesi, L. G.: Strain weakening enables continental plate tectonics, Tectonophysics, 631, 189–196, 2014.

Hacker, B. R., Peacock, S. M., Abers, G. A., and Holloway, S. D.: Subduction factory 2. Are intermediate-depth earthquakes in subducting slabs linked to metamorphic dehydration reactions?, Journal of Geophysical Research: Solid Earth, 108, 2003.

Haines, S. H., Kaproth, B., Marone, C., Saffer, D., and Van der Pluijm, B.: Shear zones in clay-rich fault gouge: A laboratory study of fabric development and evolution, Journal of Structural Geology, 51, 206–225, 2013.

Hall, S. A.: Characterization of fluid flow in a shear band in porous rock using neutron radiography, Geophysical Research Letters, 40, 2613–2618, 2013.

Holtzman, B. K.: Questions on the existence, persistence, and mechanical effects of a very small melt fraction in the asthenosphere, Geochemistry, Geophysics, Geosystems, 17, 470–484, 2016.

Hughes, A., Kendrick, J. E., Salas, G., Wallace, P. A., Legros, F., Toro, G. D., and Lavallée, Y.: Shear localisation, strain partitioning and frictional melting in a debris avalanche generated by volcanic flank collapse, Journal of Structural Geology, 140, https://doi.org/10.1016/j.jsg.2020.104132, 2020.

Hutchinson, J. W. and Tvergaard, V.: Shear band formation in plane strain, International Journal of Solids and Structures, 17, 451–470, 1981.

Jacquey, A. B. and Cacace, M.: Multiphysics modeling of a brittle-ductile lithosphere: 1. Explicit visco-elasto-plastic formulation and its numerical implementation, Journal of Geophysical Research: Solid Earth, 125, e2019JB018 474, 2020.

John, T., Medvedev, S., Rüpke, L. H., Andersen, T. B., Podladchikov, Y. Y., and Austrheim, H.: Generation of intermediate-depth earthquakes by self-localizing thermal runaway, Nature Geoscience, 2, 137–140, 2009.

Katz, R. F., Spiegelman, M., and Holtzman, B.: The dynamics of melt and shear localization in partially molten aggregates, Nature, 442, 676–679, 2006.

Kaus, B. J.: Factors that control the angle of shear bands in geodynamic numerical models of brittle deformation, Tectonophysics, 484, 36–47, https://doi.org/10.1016/j.tecto.2009.08.042, 2010.

Kelemen, P. and Hirth, G.: Periodic Viscous Shear Heating Instability in Fine-Grained Shear Zones: Possible Mechanism for Intermediate Depth Earthquakes and Slow Earthquakes?, in: AGU Fall Meeting Abstracts, vol. 2004, pp. T23A–0563, 2004.

Kelemen, P. B. and Hirth, G.: A periodic shear-heating mechanism for intermediate-depth earthquakes in the mantle, Nature, 446, 787–790, 2007.

Kirkpatrick, J. D., Fagereng, Å., and Shelly, D. R.: Geological constraints on the mechanisms of slow earthquakes, Nature Reviews Earth & Environment, 2, 285–301, 2021.

Koizumi, T., Tsunogae, T., van Reenen, D. D., Smit, C. A., and Belyanin, G. A.: Fluid migration along deep-crustal shear zone: A case study of the Rhenosterkoppies Greenstone Belt in the northern Kaapvaal Craton, South Africa, Geological Journal, 58, 3928–3947, https://doi.org/10.1002/gj.4818, 2023.

Korup, O., Clague, J. J., Hermanns, R. L., Hewitt, K., Strom, A. L., and Weidinger, J. T.: Giant landslides, topography, and erosion, Earth and Planetary Science Letters, 261, 578–589, 2007.

Kotowski, A. J. and Behr, W. M.: Length scales and types of heterogeneities along the deep subduction interface: Insights from exhumed rocks on Syros Island, Greece, Geosphere, 15, 1038–1065, 2019.

Lavier, L. L., Tong, X., and Biemiller, J.: The mechanics of creep, slow slip events, and earthquakes in mixed brittle-ductile fault zones, Journal of Geophysical Research: Solid Earth, 126, e2020JB020 325, 2021.

Lin, A.: S–C cataclasite in granitic rock, Tectonophysics, 304, 257–273, 1999.

Lister, G. and Snoke, A.: SC mylonites, Journal of Structural Geology, 6, 617–638, 1984.

Lloyd, G. E. and Kendall, J.-M.: Petrofabric-derived seismic properties of a mylonitic quartz simple shear zone: implications for seismic reflection profiling, Geological Society, London, Special Publications, 240, 75–94, 2005.

Logan, J., Dengo, C., Higgs, N., and Wang, Z.: Fabrics of experimental fault zones: Their development and relationship to mechanical behavior, in: International geophysics, vol. 51, pp. 33–67, Elsevier, 1992.

Logan, J. M.: Brittle phenomena, Reviews of Geophysics, 17, 1121–1132, 1979.

Logan, J. M. and Rauenzahn, K. A.: Frictional dependence of gouge mixtures of quartz and montmorillonite on velocity, composition and fabric, Tectonophysics, 144, 87–108, 1987.

Mair, K. and Abe, S.: 3D numerical simulations of fault gouge evolution during shear: Grain size reduction and strain localization, Earth and Planetary Science Letters, 274, 72–81, https://doi.org/10.1016/j.epsl.2008.07.010, 2008.

Malik, J. N., Murty, C., and Rai, D. C.: Landscape changes in the Andaman and Nicobar Islands (India) after the December 2004 great Sumatra earthquake and Indian Ocean tsunami, Earthquake Spectra, 22, 43–66, 2006.

Maltman, A. J.: Some microstructures of experimentally deformed argillaceous sediments, Tectonophysics, 39, 417–436, 1977.

Mancktelow, N. S.: How ductile are ductile shear zones?, Geology, 34, 345–348, https://doi.org/10.1130/G22260.1, 2006.

Mancktelow, N. S., Camacho, A., and Pennacchioni, G.: Time-Lapse Record of an Earthquake in the Dry Felsic Lower Continental Crust Preserved in a Pseudotachylyte-Bearing Fault, Journal of Geophysical Research: Solid Earth, 127, https://doi.org/10.1029/2021JB022878, 2022.

Mansour, J., Giordani, J., Moresi, L., Beucher, R., Kaluza, O., Velic, M., Farrington, R., Quenette, S., and Beall, A.: Underworld2: Python geodynamics modelling for desktop, HPC and cloud, Journal of Open Source Software, 5, 1797, 2020.

Marone, C. and Scholz, C.: Particle-size distribution and microstructures within simulated fault gouge, Journal of Structural Geology, 11, 799–814, 1989.

Marone, C., Raleigh, C. B., and Scholz, C.: Frictional behavior and constitutive modeling of simulated fault gouge, Journal of Geophysical Research: Solid Earth, 95, 7007–7025, 1990.

Marques, F., Burg, J.-P., Armann, M., and Martinho, E.: Rheology of synthetic polycrystalline halite in torsion, Tectonophysics, 583, 124–130, 2013.

Mazumder, R., Van Loon, A., Mallik, L., Reddy, S., Arima, M., Altermann, W., Eriksson, P., and De, S.: Mesoarchaean–Palaeoproterozoic stratigraphic record of the Singhbhum crustal province, eastern India: a synthesis, Geological Society, London, Special Publications, 365, 31–49, 2012.

Menegon, L., Campbell, L., Mancktelow, N., Camacho, A., Wex, S., Papa, S., Toffol, G., and Pennacchioni, G.: The earthquake cycle in the dry lower continental crust: insights from two deeply exhumed terranes (Musgrave Ranges, Australia and Lofoten, Norway), Philosophical transactions of the Royal Society A, 379, 20190 416, 2021.

Meyer, S. E., Kaus, B. J., and Passchier, C.: Development of branching brittle and ductile shear zones: A numerical study, Geochemistry, Geophysics, Geosystems, 18, 2054–2075, 2017.

Mildon, Z. K., Roberts, G. P., Faure Walker, J. P., Beck, J., Papanikolaou, I., Michetti, A. M., Toda, S., Iezzi, F., Campbell, L., McCaffrey, K. J., et al.: Surface faulting earthquake clustering controlled by fault and shear-zone interactions, Nature Communications, 13, 7126, 2022.

Misra, S., Burlini, L., and Burg, J. P.: Strain localization and melt segregation in deforming metapelites, Physics of the Earth and Planetary Interiors, 177, 173–179, https://doi.org/10.1016/j.pepi.2009.08.011, 2009.

Moresi, L., Quenette, S., Lemiale, V., Meriaux, C., Appelbe, B., and Mühlhaus, H.-B.: Computational approaches to studying non-linear dynamics of the crust and mantle, Physics of the Earth and Planetary Interiors, 163, 69–82, 2007.

Morgenstern, N. and Tchalenko, J.: Microstructural observations on shear zones from slips in natural clays, 1967.

Mukherjee, S. and Koyi, H. A.: Higher Himalayan Shear Zone, Zanskar Indian Himalaya: microstructural studies and extrusion mechanism by a combination of simple shear and channel flow, International Journal of Earth Sciences, 99, 1083–1110, 2010.

Mukhopadhyay, D. and Deb, G. K.: Structural and textural development in Singhbhum shear zone, eastern India, Proceedings of the Indian Academy of Sciences-Earth and Planetary Sciences, 104, 385–405, 1995.

Mukhopadhyay, M., Roy, A., and Mandal, N.: Mechanisms of Shear Band Formation in Heterogeneous Materials Under Compression: The Role of Pre-Existing Mechanical Flaws, Journal of Geophysical Research (Solid Earth), 128, e2022JB026 169, 2023.

Niemeijer, A. and Spiers, C.: Velocity dependence of strength and healing behaviour in simulated phyllosilicate-bearing fault gouge, Tectonophysics, 427, 231–253, 2006.

Niemeijer, A. R. and Spiers, C. J.: Influence of phyllosilicates on fault strength in the brittle-ductile transition: Insights from rock analogue experiments, Geological Society, London, Special Publications, 245, 303–327, 2005.

Okamoto, A. S., Verberne, B. A., Niemeijer, A. R., Takahashi, M., Shimizu, I., Ueda, T., and Spiers, C. J.: Frictional properties of simulated chlorite gouge at hydrothermal conditions: Implications for subduction megathrusts, Journal of Geophysical Research: Solid Earth, 124, 4545–4565, 2019.

Ord, A., Hobbs, B., and Regenauer-Lieb, K.: Shear band emergence in granular materials - A numerical study, International Journal for Numerical and Analytical Methods in Geomechanics, 31, 373–393, https://doi.org/10.1002/nag.590, 2007.

https://doi.org/10.5194/egusphere-2024-1077
Preprint. Discussion started: 22 April 2024

Orellana, L., Scuderi, M., Collettini, C., and Violay, M.: Frictional properties of Opalinus Clay: Implications for nuclear waste storage, Journal of Geophysical Research: Solid Earth, 123, 157–175, 2018.

Papa, S., Pennacchioni, G., Camacho, A., and Larson, K. P.: Pseudotachylytes in felsic lower-crustal rocks of the Calabrian Serre massif: A record of deep-or shallow-crustal earthquakes?, Lithos, 460, 107 375, 2023.

Passchier, C. W. and Trouw, R. A.: Microtectonics, Springer Science & Business Media, 2005.

Paterson, M. S. and Wong, T.-f.: Experimental rock deformation: the brittle field, vol. 348, Springer, 2005.

Pennacchioni, G. and Mancktelow, N.: Small-scale ductile shear zones: neither extending, nor thickening, nor narrowing, Earth-Science Reviews, 184, 1–12, 2018.

Platt, J. P., Xia, H., and Schmidt, W. L.: Rheology and stress in subduction zones around the aseismic/seismic transition, Progress in Earth and Planetary Science, 5, 1–12, 2018.

Précigout, J., Prigent, C., Palasse, L., and Pochon, A.: Water pumping in mantle shear zones, Nature Communications, 8, 15 736, 2017.

Ramsay, J. G., Huber, M. I., and Lisle, R. J.: The techniques of modern structural geology: Folds and fractures, vol. 2, Academic press, 1983.

Ranalli, G.: Rheology of the Earth, Springer Science & Business Media, 1995.

Ranalli, G.: Rheology of the lithosphere in space and time, Geological Society, London, Special Publications, 121, 19–37, 1997.

Rast, M. and Ruh, J. B.: Numerical shear experiments of quartz-biotite aggregates: Insights on strain weakening and two-phase flow laws, Journal of Structural Geology, 149, 104 375, 2021.

Reber, J. E., Lavier, L. L., and Hayman, N. W.: Experimental demonstration of a semi-brittle origin for crustal strain transients, Nature Geoscience, 8, 712–715, 2015.

Rice, J. R.: Heating and weakening of faults during earthquake slip, Journal of Geophysical Research: Solid Earth, 111, 2006.

Rodriguez Padilla, A. M.: Decoding earthquake mechanics with repeat pass airborne lidar, Nature Reviews Earth & Environment, 4, 355–355, 2023.

Rodriguez Padilla, A. M., Oskin, M. E., Milliner, C. W., and Plesch, A.: Accrual of widespread rock damage from the 2019 Ridgecrest earthquakes, Nature Geoscience, 15, 222–226, 2022.

Roscoe, K. H.: The influence of strains in soil mechanics, Geotechnique, 20, 129–170, 1970.

Roy, A., Roy, N., Saha, P., and Mandal, N.: Factors Determining Shear-Parallel Versus Low-Angle Shear Band Localization in Shear Deformations: Laboratory Experiments and Numerical Simulations, Journal of Geophysical Research: Solid Earth, 126, e2021JB022 578, 2021.

Roy, A., Ghosh, D., and Mandal, N.: Dampening effect of global flows on Rayleigh–Taylor instabilities: implications for deep-mantle plumes vis-à-vis hotspot distributions, Geophysical Journal International, 236, 119–138, 2024.

Roy, N., Roy, A., Saha, P., and Mandal, N.: On the origin of shear-band network patterns in ductile shear zones, Proceedings of the Royal Society A, 478, 20220 146, 2022.

Rudnicki, J. W. and Rice, J.: Conditions for the localization of deformation in pressure-sensitive dilatant materials, Journal of the Mechanics and Physics of Solids, 23, 371–394, 1975.

Ruggieri, R., Scuderi, M. M., Trippetta, F., Tinti, E., Brignoli, M., Mantica, S., Petroselli, S., Osculati, L., Volontè, G., and Collettini, C.: The role of shale content and pore-water saturation on frictional properties of simulated carbonate faults, Tectonophysics, 807, 228 811, 2021.

Rutter, E., Maddock, R., Hall, S., and White, S.: Comparative microstructures of natural and experimentally produced clay-bearing fault gouges, Pure and applied geophysics, 124, 3–30, 1986.

https://doi.org/10.5194/egusphere-2024-1077
Preprint. Discussion started: 22 April 2024

Saffer, D. M. and Marone, C.: Comparison of smectite-and illite-rich gouge frictional properties: application to the updip limit of the seismogenic zone along subduction megathrusts, Earth and Planetary Science Letters, 215, 219–235, 2003.

Sandiford, D. and Moresi, L.: Improving subduction interface implementation in dynamic numerical models, Solid Earth, 10, 969–985, 2019.

Schueller, S., Gueydan, F., and Davy, P.: Mechanics of the transition from localized to distributed fracturing in layered brittle-ductile systems, Tectonophysics, 484, 48–59, https://doi.org/10.1016/j.tecto.2009.09.008, 2010.

Shimamoto, T.: Transition between frictional slip and ductile flow for halite shear zones at room temperature, Science, 231, 711–714, 1986.

Shimamoto, T.: The origin of SC mylonites and a new fault-zone model, Journal of Structural Geology, 11, 51–64, 1989.

Sibson, R. H.: Generation of pseudotachylyte by ancient seismic faulting, Geophysical Journal International, 43, 775–794, 1975.

Sibson, R. H.: Fault rocks and fault mechanisms, Journal of the Geological Society, 133, 191–213, https://doi.org/10.1144/gsjgs.133.3.0191, 1977.

Spruzeniece, L. and Piazolo, S.: Strain localization in brittle–ductile shear zones: fluid-abundant vs. fluid-limited conditions (an example from Wyangala area, Australia), Solid Earth, 6, 881–901, 2015.

Tesei, T., Collettini, C., Carpenter, B. M., Viti, C., and Marone, C.: Frictional strength and healing behavior of phyllosilicate-rich faults, Journal of Geophysical Research: Solid Earth, 117, 2012.

Tesei, T., Collettini, C., Barchi, M. R., Carpenter, B. M., and Di Stefano, G.: Heterogeneous strength and fault zone complexity of carbonate-bearing thrusts with possible implications for seismicity, Earth and Planetary Science Letters, 408, 307–318, 2014.

Thielmann, M. and Kaus, B. J.: Shear heating induced lithospheric-scale localization: Does it result in subduction?, Earth and Planetary Science Letters, 359, 1–13, 2012.

Tokle, L., Hirth, G., and Stünitz, H.: The effect of muscovite on the microstructural evolution and rheology of quartzite in general shear, Journal of Structural Geology, 169, https://doi.org/10.1016/j.jsg.2023.104835, 2023.

Torki, M. E. and Benzerga, A. A.: A mechanism of failure in shear bands, Extreme mechanics letters, 23, 67–71, 2018.

Tulley, C. J., Fagereng, Ujiie, K., Diener, J. F., and Harris, C.: Embrittlement Within Viscous Shear Zones Across the Base of the Subduction Thrust Seismogenic Zone, Geochemistry, Geophysics, Geosystems, 23, https://doi.org/10.1029/2021GC010208, 2022.

Ujiie, K., Saishu, H., Fagereng, Å., Nishiyama, N., Otsubo, M., Masuyama, H., and Kagi, H.: An explanation of episodic tremor and slow slip constrained by crack-seal veins and viscous shear in subduction mélange, Geophysical Research Letters, 45, 5371–5379, 2018.

Vardoulakis, I., Goldscheider, M., and Gudehus, G.: Formation of shear bands in sand bodies as a bifurcation problem, International Journal for numerical and analytical methods in Geomechanics, 2, 99–128, 1978.

Vauchez, A., Tommasi, A., and Mainprice, D.: Faults (shear zones) in the Earth's mantle, Tectonophysics, 558, 1–27, 2012.

Vissers, R. L., Ganerød, M., Pennock, G. M., and van Hinsbergen, D. J.: Eocene seismogenic reactivation of a Jurassic ductile shear zone at Cap de Creus, Pyrenees, NE Spain, Journal of Structural Geology, 134, 103 994, 2020.

Volpe, G., Pozzi, G., and Collettini, C.: YBPR or SCC′? Suggestion for the nomenclature of experimental brittle fault fabric in phyllosilicate-granular mixtures, Journal of Structural Geology, 165, 104 743, 2022.

Wang, J., Howarth, J. D., McClymont, E. L., Densmore, A. L., Fitzsimons, S. J., Croissant, T., Gröcke, D. R., West, M. D., Harvey, E. L., Frith, N. V., et al.: Long-term patterns of hillslope erosion by earthquake-induced landslides shape mountain landscapes, Science Advances, 6, eaaz6446, 2020.

Wang, Q. and Lade, P. V.: Shear banding in true triaxial tests and its effect on failure in sand, Journal of engineering mechanics, 127, 754–761, 2001.

Wijeyesekera, D. C. and De Freitas, M.: High-Pressure Consolidation of Kaolinitic Clay: GEOLOGIC NOTES, AAPG Bulletin, 60, 293–298, 1976.

Wu, G. and Lavier, L. L.: The effects of lower crustal strength and preexisting midcrustal shear zones on the formation of continental core complexes and low-angle normal faults, Tectonics, 35, 2195–2214, 2016.